Available online at www.sciencedirect.com

ScienceDirect

Underground Space 7 (2022) 944–965

www.keaipublishing.com/undsp

Numerical investigation on arching effect surrounding deep cylindrical shaft during excavation process

Tanawat Tangjarusritaratorn [a,*], Yuusuke Miyazaki [a], Yasuo Sawamura [a]
Kiyoshi Kishida [a], Makoto Kimura [b]

[a] *Dept. of Urban Management, Kyoto Univ., Katsura Campus, Kyoto 615-8540, Japan*
[b] *Dept. of Civil and Earth Resources Engineering, Kyoto Univ., Katsura Campus, Kyoto 615-8540, Japan*

Received 2 June 2021; received in revised form 19 November 2021; accepted 1 January 2022
Available online 19 March 2022

Abstract

Predicting the inner displacements of deep vertical shafts during the excavation process has been a difficult task considering the geological, structural, and constructional influences. In fact, the two-dimensional (2D) analytical solution based on the retaining wall model remains insufficient for understanding the actual behavior during an excavation. This is because the deformation of vertical shafts becomes complicated due to the unexpected arching effect brought about by the three-dimensional (3D) flexible displacements occurring in the excavation process. Previous analytical solutions only considered the limit equilibrium. Therefore, the present study deals with a 3D soil-structure simulation by considering the displacements of a cylindrical shaft and the mechanical behavior of the surrounding soil as well as the geometry of the cylindrical structure. Moreover, this mechanical behaviors of the surrounding soil and shaft are controlled by the shaft stiffness; hence, the relationships among the shaft stiffness, mechanical behavior of the surrounding soil (in terms of earth pressure coefficient), and shaft displacement were investigated. A cylindrical model, 120 m in depth and 20 m in diameter, was positioned at the center of a sand domain, and each excavation step was performed at an interval depth of 20 m. A 3D finite difference method analysis was applied using the modified Cam-Clay (MCC) model to represent the soil behavior. As a result, the present study provides a new normalized lateral earth pressure theory for excavated shafts by considering the 3D arching effect obtained from parametric studies using various levels of shaft stiffness. From a comparison with the analytical solutions of previous studies (Terzaghi, 1943a; Prater, 1977; Cheng & Hu, 2005), it is found that the previous studies underestimated the earth pressure acting on the cylindrical shaft because they did not consider the accurate arching effect.

Keywords: Deep cylindrical shaft; Excavation analysis; Soil mixing wall method; Arching effect; Finite different method; Three-dimensional analysis

1 Introduction

In recent years, cylindrical shaft construction has become popular for several reasons: the ventilation system, the emergency exits, and the temporary structure it provides during the tunneling construction, in accordance with the advantageous structural geometry. In addition, a deep shaft structure is preferred to a shallow shaft structure in order to avoid any existing underground structures, which could cause ground movement and change the stress state in the sub-soil (Ng et al., 2018).

The utilization of a cylindrical vertical shaft is always accompanied by a complex phenomenon, namely, the arching effect (Liu, 2014). The arching effect occurs when stress is transferred due to the uniform deformation caused by relative movement (Terzaghi, 1943a). The famous model used to investigate the arching effect is the trapdoor model; it is represented by either a numerical model or a physical model (Nakai et al., 1997; Lai et al., 2018; Rui et al., 2018). Depending on the uniform load and the deformation of the

* Corresponding author.
E-mail address: tangjarusritaratorn.tanawat.w16@kyoto-u.jp (T. Tangjarusritaratorn).

https://doi.org/10.1016/j.undsp.2022.01.004

cylindrical shaft during an excavation, the arching effect might play a key role in the mechanical behavior of the soil.

Numerical approaches, physical models, and in situ tests have mainly been used to clarify the mechanical behavior of the soil surrounding a cylindrical shaft during the excavation process. Some researchers have observed the cylindrical shaft behavior during construction and noted that cylindrical shaft deformation is basically different from the conventional deformation of retaining walls (Muramatsu & Abe, 1996; Tan & Wang, 2013; Aye et al., 2014; Tan et al., 2018). Moreover, Kim et al. (2013) observed the earth pressure distribution in full-scale tests, which showed a decline in earth pressure due to the increase in depth. Hence, the mechanical behavior of the surrounding soil along a cylindrical shaft is also likely to be different from that of the retaining wall structure. Kim et al. (2013) used physical modeling to try to clarify the earth pressure distribution along a cylindrical shaft by creating artificial displacements, for which the earth pressure distribution seemed to be different from that of the theoretical solution. Numerical modeling is also one of the approaches for clarifying the mechanical behaviors of the surrounding soil and the cylindrical shaft after an excavation. Prior to the current study, most of the numerical simulations of cylindrical shaft problems were done by 2D axisymmetric simulations (Cheng et al., 2007; Cho et al., 2015; Meftah et al., 2018). According to the prominence of the three-dimensional effect on the cylindrical shaft simulation, Chehadeh et al. (2019) used a 3D finite element analysis to show the distribution of earth pressure on a cylindrical shaft.

It is well known that the phenomenon of the soil behavior surrounding cylindrical shafts is associated with the arching effect, in which lateral earth pressure will experience compression and extension in tangential and radial directions, respectively. Several analytical solutions have been proposed to estimate the earth pressure acting on a cylindrical shaft. Most of the analytical solutions were based on the limit equilibrium or slip-line method (Tobar & Meguid, 2010). Prater (1977) suggested a solution based on the limit equilibrium method, in which the earth pressure tends to decrease at deeper locations. Likewise, Terzaghi (1943b) used the equilibrium of a slipping soil wedge to estimate the earth pressure with the axisymmetric method (Terzaghi, 1943b; Prater, 1977). Conversely, Berezantev (1958) and Cheng and Hu (2005) proposed solutions based on applying the slip-line method in the axisymmetric method (Berezantev, 1958; Cheng & Hu, 2005). Nevertheless, neither the limit equilibrium nor the slip-line method could rigorously assess the earth pressure while considering the real displacements.Furthermore, the stress–strain for the cylindrical coordinate relationship, shown in Eq. (1), is ignored in the slip-line method. In addition, the failure surface must be assumed in the limit equilibrium method (Prater, 1977; Liu & Wang, 2008; Cheng et al., 2016; Xiong et al., 2019).

$$\frac{\partial \dot{\varepsilon}_\theta}{\partial r} - \frac{\dot{\varepsilon}_r - \dot{\varepsilon}_\theta}{r} = f_r, \tag{1}$$

where $\dot{\varepsilon}_\theta$ and $\dot{\varepsilon}_r$ are the strain rates in the tangential and radial directions, respectively, r is the radial length from axis of symmetry in cylindrical coordinate and f_r is radial component of body force, which is 0 for static equilibrium.

In general, the earth pressure acting on a vertical structure can develop and change due to the wall displacement (movement). An excavation is one of the key factors in the generation of displacement. In the same manner, there is a phenomenon of earth pressure acting on the cylindrical shaft due to the excavation. Moreover, different excavation sequences influence the development of earth pressure along the cylindrical shaft in different ways. The earth pressure coefficient may be uncertain depending on the different types of soil behavior found at each depth.

The underground structures could be constructed by several methods depending on their characteristics. A deep shaft or retaining wall is generally constructed by the soil mixing wall (SMW) method or the cement deep mixing (CDM) method, as shown in Fig. 1, firstly developed by the Seiko Kogyo Company (Bruce, 2000; David & Yang, 2003). According to the SMW construction method, the original ground is blended with a cementitious material to increase the strength (Bruce, 2013a). The strength of deep mixed soil, therefore, depends on the type of binder, the soil properties, the mixing conditions, and even the curing conditions (Bruce, 2013b). Imamura et al. (2000) conducted centrifuge experiments to investigate the earth pressure acting on a cylindrical shaft with different uniform displacements to show that the development of earth pressure significantly depends on the displacement (Imamura et al., 2000). It was found that the different amounts of deformation due to the variation in shaft stiffness will cause a difference in the mechanical behavior of the soil.

According to the cylindrical shaft construction by using the SMW method, the surrounding soil and shaft lining would undergo arching effect and uncertain earth pressure, respectively. Therefore, it is difficult to estimate the horizontal earth pressure acting on the shaft in the design phase due to the unknown generation of the arching effect. Additionally, the arching effect is likely to be generated by the wall deformation itself. However, the wall deformation of a vertical shaft is controlled by the structural characteristics of the vertical shaft construction method. And, the effects of the various wall deformation modes on the arching effect remain unclear. This necessitates a fundamental verification of the mechanism that generates the arching effect along with the various patterns of shaft deformation.

Hence, the objective of this paper is to clarify the mechanism that generates the development of the arching effect surrounding deep cylindrical shafts induced by various amounts of inner wall deformation. In addition, the construction sequence, wall installation procedure, and excavation process are included in order to follow a real construction based on the SMW method. The arching

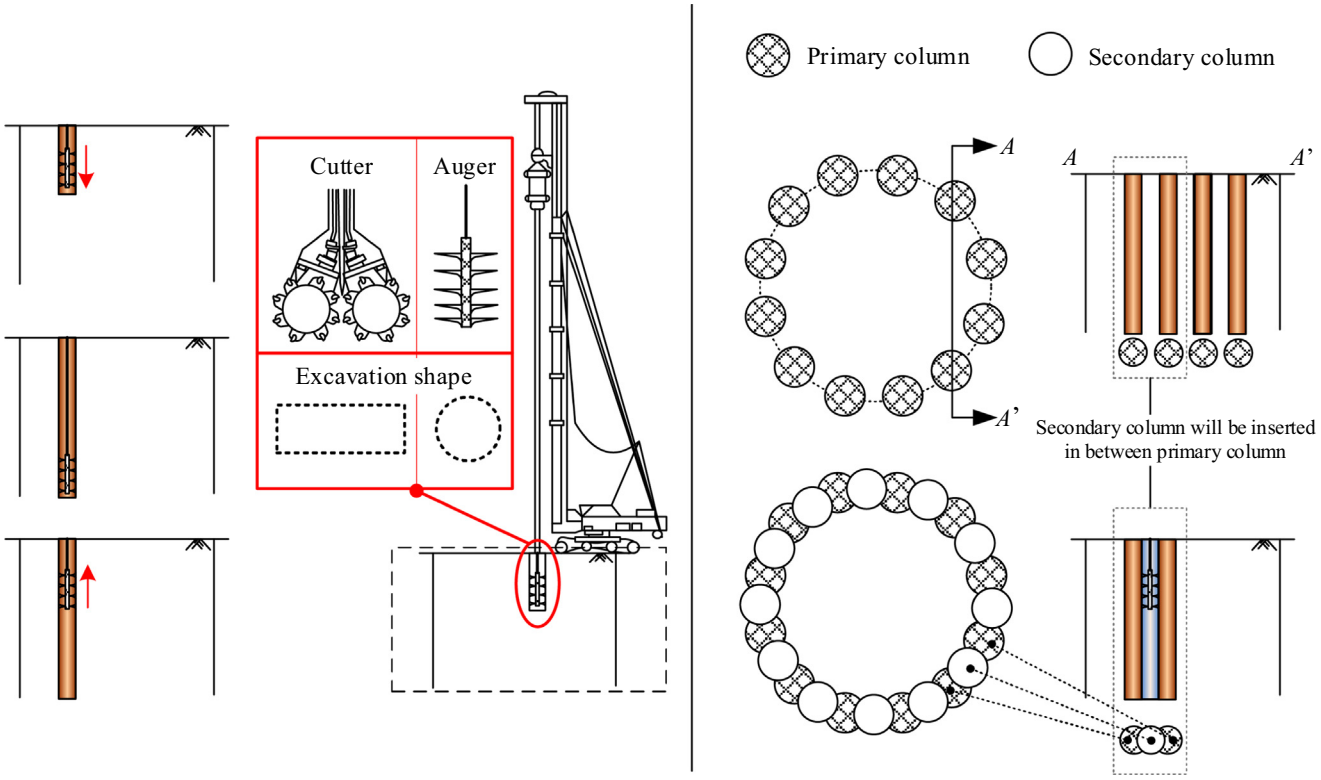

Fig. 1. Construction processes of the SMW and CDM methods.

effect surrounding a cylindrical shaft is firstly elucidated, and then the earth pressure distribution along the cylindrical shaft is clarified.

2 Numerical modelling

2.1 Model description

The finite difference method was utilized in the FLAC3D formulation to simulate a cylindrical vertical shaft during the excavation process (Itasca Consulting Group, 2017). The simulation employed the typical construction process and dimensions. Using twenty-one samples for the shaft construction, Muramatsu and Abe (1996) summarized the dimensions of a deep vertical shaft as well as the excavation depth that were typically employed in Japanese shaft construction in those days. According to their report, deep cylindrical shafts were generally about 120 m in length and 80 m in excavation depth. In addition, cylindrical shafts were generally constructed to have a diameter of 20 m.

The cylindrical shaft dimensions for this study were determined after giving careful consideration to the diameter, length, excavation depth, and thickness, as shown in Fig. 2. The values correspond to those used in a real construction. The excavation process inside the cylindrical shaft was divided into four steps with excavation steps of 20 m each. In addition, the stress relaxation and mesh removal method as shown in Fig. 3, which is a tunneling modeling method, was utilized in this analysis (Dias & Kastner, 2013; Sun & Dias, 2019).

The main issue to determine the size of the domain is stress distortion, which is the most prominent error commonly occurring in the simulation. The stress distortion appearing in a simulation is generally influenced by the small size of the domain. Therefore, a proper domain size should be used in order to prevent erroneous results. A simplified solution for the stress surrounding the borehole should be selected to represent the worst-case scenario of stress distortion on the horizontal plane. Several solutions for the borehole problem have been suggested in a function of borehole radius, R_W. In addition, the stress changes in both radial and tangential directions depend on the distance in radial direction, r (Fjar et al., 2008). The simplest solution, based on the equilibrium equation for the cylindrical coordinates, was selected as seen in Eqs. (2) to (5). The influence of the borehole on the stress of the surrounding soil is shown in Fig. 4, where the stress variations in both radial and tangential directions are lower than 5% at $5.0R_W$, namely,

$$\sigma_r = \sigma_0 + \Delta\sigma_r, \tag{2}$$

$$\Delta\sigma_r = -(\sigma_h - p_w)\left(\frac{R_W}{r}\right)^2, \tag{3}$$

$$\sigma_\theta = \sigma_0 + \Delta\sigma_\theta, \tag{4}$$

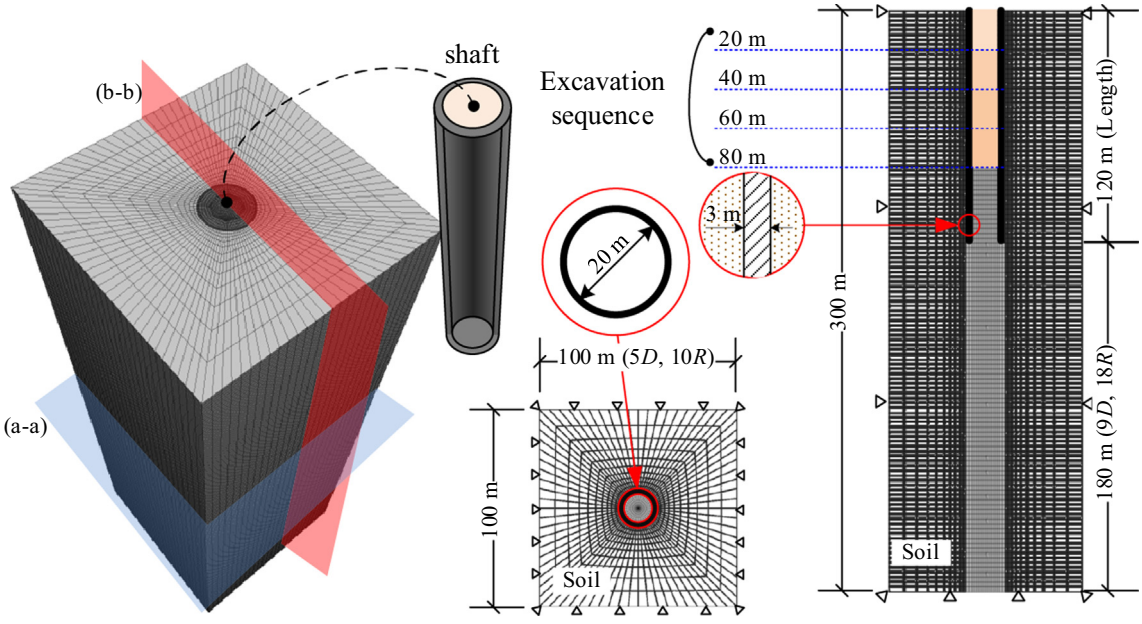

(a) Simulation Model (b) Top view (a-a) (c) Side view (b-b)

Fig. 2. Schematic section of circular shaft model.

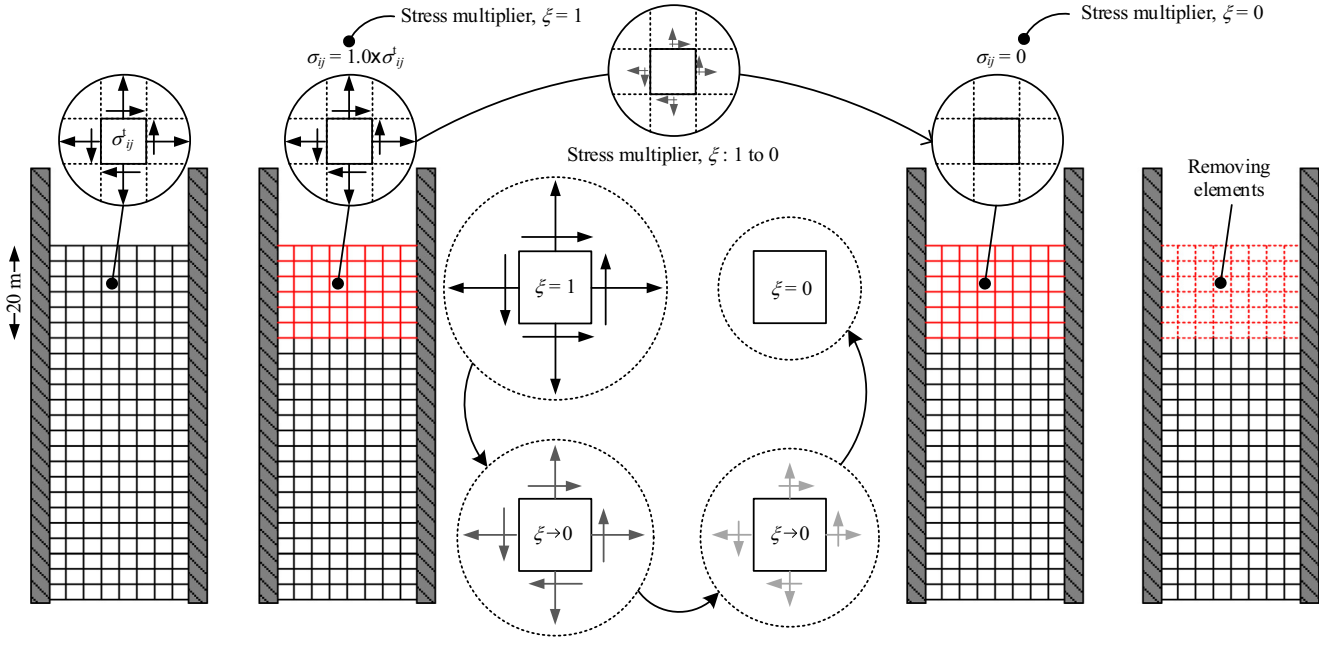

Fig. 3. Excavation process in numerical simulation.

$$\Delta\sigma_\theta = (\sigma_h - p_w)\left(\frac{R_W}{r}\right)^2, \tag{5}$$

where σ_r is the radial stress, σ_θ is the tangential stress, σ_h is the horizontal stress, R_W is the borehole radius, r is the distance from the center of the borehole, and p_w is the water pressure inside the borehole.

The Boussinesq solution was applied to estimate the variation in vertical stress influenced by a uniformly loaded circular area, as shown in Eq. (6) (Das, 2013a). Figure 5 shows increments in vertical stress, $\Delta\sigma_z$, in the subsoil, where the value of $\frac{\Delta\sigma_z}{q}$ is less than 0.5% at the normalized depth, $\frac{z}{R}$, equal to 18.

$$\Delta\sigma_z = q\left\{1 - \frac{1}{\left[\left(\frac{R}{z}\right)^2 + 1\right]^{3/2}}\right\}, \tag{6}$$

where q is the load per unit area, σ_z is the vertical stress, R is the load radius, and z is the depth.

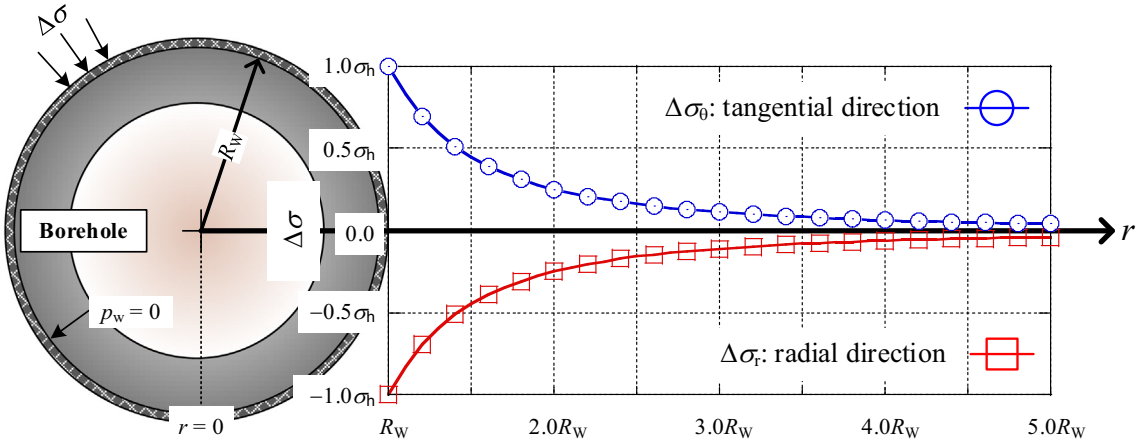

Fig. 4. Stress distribution around borehole in linear elastic formation.

To simulate the procedure, the first step is to assign initial stress all over the domain by considering its density, gravity, and at-rest earth pressure coefficient, K_0, which is basically a function of internal friction angle as following Fig. 6. However, the constitutive model of soil material is modified Cam-Clay (MCC) model, therefore, the initial stress might not be the exact stress because MCC model does not really consider and require internal friction angle. Hence, the self-weight analysis will complete the stress initialization of ground entire domain. Next, the process of shaft installation, the constitutive model, namely, the elastic model, and the parameters for the shaft were used for the shaft structure instead of the MCC model. Afterward, the execution of the self-weight analysis was conducted again. Finally, the excavation sequence was carried out to show the shaft deformation, lateral earth pressure, earth pressure coefficient, etc.

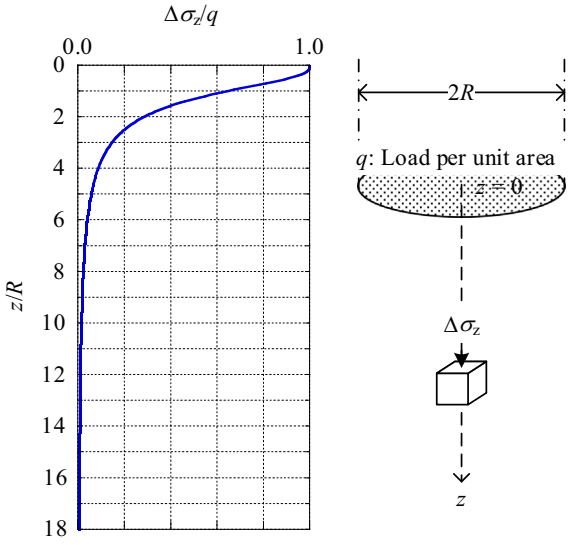

Fig. 5. Influence of uniformly loaded circular area on vertical stress.

2.2 Constitutive model and input parameters

According to the aim of this research, the excavation inside a deep cylindrical shaft is in our interest. When conducting a cylindrical shaft analysis with the deep excavation process, the constitutive model must satisfy the depth effect (pressure dependency). The MCC model, an elasto-plastic model, is one of the famous constitutive models that can represent the significant mechanical behavior, for instance, the hardening/softening behavior. In addition, the MCC model has been widely used in several applications including excavations behind retaining walls (Hashash et al., 2003; Salman et al., 2011; Hsieh et al., 2012; Jiang et al., 2013; Nunez et al., 2013; Goh & Mair, 2014; Tang et al., 2018). The pressure dependency has already been considered in the MCC model with the tangential bulk modulus, $K = \frac{\Delta p}{\Delta \epsilon_p^e}$, for elastic volumetric changes (Wood, 1990; Itasca Consulting Group, 2017), as shown in Eq. (7):

$$\Delta p = \frac{vp}{\kappa} \Delta \epsilon_p^e, \tag{7}$$

where p is the mean effective pressure, v is the specific volume, $\Delta \epsilon_p^e$ is the change in elastic volumetric strain, and κ is the swelling index.

Salman et al. (2011) and Jiang et al. (2013) used an elastic model to represent the retaining wall in their numerical simulations (Salman et al., 2011; Jiang et al., 2013). Likewise, Zhang and Chen (2019) used an elastic model in his dynamic simulation of a cylindrical shaft. In the present study, therefore, the isotropic elastic model was employed to represent the mechanical behavior of the cylindrical shaft (Zhang & Chen, 2019). The variation in the shaft modulus (stiffness) was included in this analysis in accordance with the soil mixing wall construction method. Furthermore, the elastic modulus of the soil mixing wall varied in the range of 10^8 to 10^{11} Pa (Fan et al., 2018). The aim of this analysis was to consider the homogeneous material (soil) undergoing the arching effect. In addition, the con-

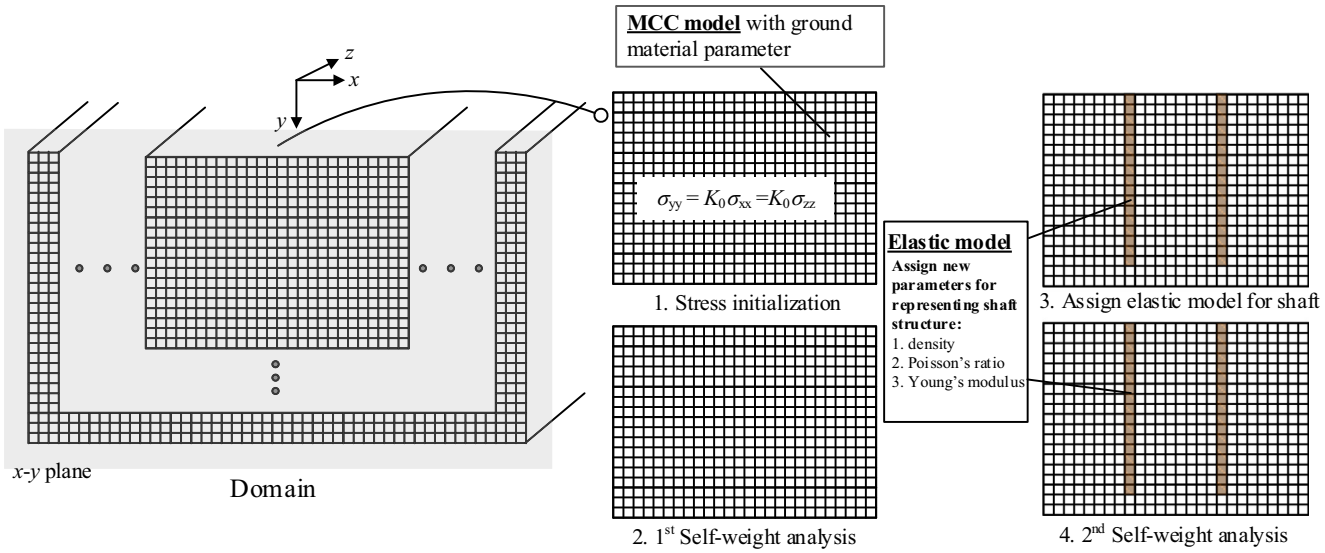

Fig. 6. Numerical simulation procedure.

Table 1
Cylindrical shaft parameters.

Isotropic elastic model	
Density (g/cm^3)	2.20
Poisson's ratio,v	0.33
Young's modulus, E (Pa)	10^8-10^{11}

Table 2
Soil parameters.

MCC model	
Maximum elastic bulk modulus, K_{max} (GPa)	5.0
Density (g/cm^3)	1.6
Swelling index,κ	0.0045
Normal consolidation line slope,λ	0.07
Poisson's ratio,v	0.33
Frictional constant,M	1.36
OCR (over-consolidation ratio)	2.0
Specific pressure at reference point, P_1 (KPa)	98.0
Specific volume at reference point, V_1	2.1

crete parameters of one of the well-known soils, Toyoura sand, have been employed in many research works (Nakai et al., 2011; Aglipay, 2015), and therefore, have also been applied in this analysis. Tables 1 and 2 show the material parameters of the structure (cylindrical shaft) and the ground, respectively. Moreover, the calculation of the triaxial simulations under monotonic loading was conducted to show the mechanical behavior of the soil represented by the MCC model, as shown in Fig. 7.

3 Parametric studies on excavation analysis

The horizontal arching effect may play a key role in the decrease in earth pressure acting on a cylindrical shaft during the excavation depending on the uniform radial displacement. Furthermore, the development of earth pressure behind the shaft wall can be influenced by the vertical arching effect due to the frictional wall (Handy, 1985; Paik & Salgado; 2003). The separation between wall and soil mass induces a downward movement of soil mass, therefore, the half arch could be defined between wall and failure line. Therefore, the arching effect brought about by the earth pressure acting on a cylindrical shaft consists of two types, vertical arching and horizontal arching, as seen in Fig. 8. Therefore, in this current study, the friction interface between surrounding soil and shaft wall is still not considered, since, the vertical arching effect might occur which could cause a disturbance on horizontal arching effect illustration.

The arching effect is generated in the surrounding soil after the excavation has been completed and has caused the deformation of the cylindrical shaft; the inner-displacement of the cylindrical shaft is induced by the uniform movement of the surrounding soil. According to this mechanism, the wall displacement not only influences the soil movement, but the generation of stress in the soil as well. Therefore, a preliminary analysis should be done to reveal the tendencies of the earth pressure and the wall displacement along the cylindrical shaft that may occur during the excavation with the application of various levels of stiffness in the shaft.

Nevertheless, an analysis of the deep cylindrical shaft, with the interface along the shaft wall and the soil, was carried out in advance to clarify the influence of the friction along the interface between the shaft and the soil. Figure 9 shows the normalized lateral earth pressure results, the ratio of lateral earth pressure to unit weight of soil, γ, and to shaft radius, R, at the final excavation, an excavation of 80 m. In addition, this analysis was simulated with the shaft, with a Young's modulus of the wall of 10 GPa. According to the zero thickness of the interface, the high value of 10 GPa was assigned as the value for both normal stiffness k_n and shear stiffness k_s of the interface. The results

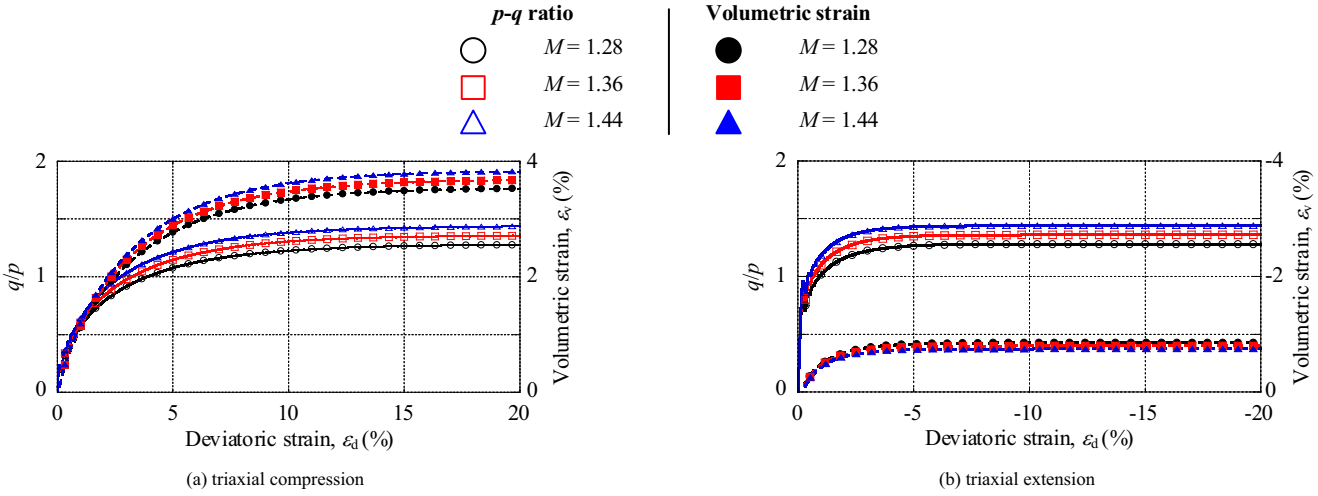

Fig. 7. Results of triaxial simulation under monotonic loading using MCC model.

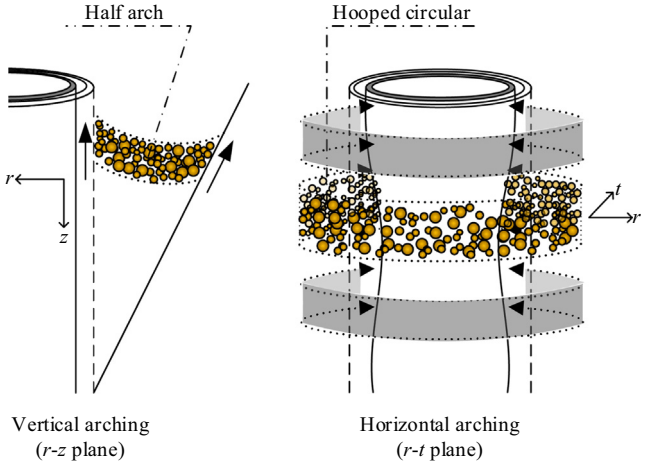

Fig. 8. Arching effect along cylindrical shaft.

show that the influence obtained by giving consideration to the interface friction causes a slight change in the lateral earth pressure. Therefore, no consideration will be given to the frictional interface in this current research work.

3.1 Fundamental behavior of cylindrical vertical shaft during the excavation process

In order to investigate the mechanisms of cylindrical shaft and surrounding soil during excavation process, three main preliminary results must be clarified before moving on a further investigation. The simulation of a cylindrical shaft during the excavation process was carried out initially with three different levels of stiffness of the shaft wall. The final depth of the excavation was 80 m from the ground surface; in addition, the excavation process was divided

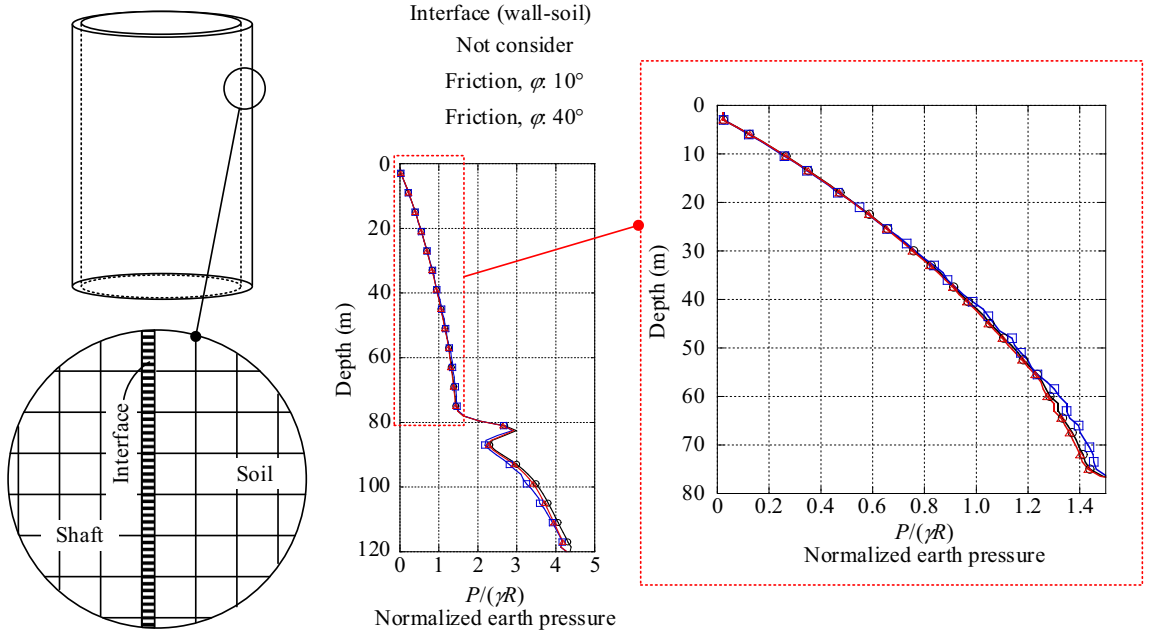

Fig. 9. Lateral earth pressure from friction wall analysis.

into four main steps (20 m, 40 m, 60 m, and 80 m), shown in Figs. 10–13, respectively. The fundamental results are composed of the wall displacement, the lateral earth pressure acting on the cylindrical shaft, and the lateral earth pressure coefficient.

Wall displacement (inner displacement): The wall displacement has been shown in terms of the real displacement, δ, and the normalized displacement, δ/*R*, which is a ratio of the inner displacement to the initial shaft radius, *R*. In most instances, the wall displacement gradually increases from the top to 10 m to 20 m above the excavation surface where the maximum displacement is located. After the final excavation, the wall displacement of the soft (flexible) cylindrical shaft, with a Young's modulus of the wall of 0.1 GPa or 100 MPa, is about 20 mm. Conversely, the wall displacement of the rigid cylindrical shaft, with a Young's modulus of the wall of 10 GPa, is less than 5 mm, as shown in Fig. 13.

Lateral earth pressure: The decrease in earth pressure above the excavation surface corresponds to the wall deformation. Nevertheless, the earth pressure acting on the cylindrical shaft goes completely against the active earth pressure theory, which leads to an unfamiliar earth pressure pattern, especially in the case of the final excavation, as shown in Fig. 13. For example, the lateral earth pressure acting on a cylindrical shaft having a Young's modulus of the wall of 1 GPa is quite similar to the active earth pressure, as seen in Figs. 7 to 9. However, the results after the final excavation show that the earth pressure at a deep position has fallen below the active earth pressure line, as presented in Fig. 13.

Earth pressure coefficient: The earth pressure coefficient, $K = \frac{\sigma_h}{\sigma_v}$, was defined by Lambe and Whitman (1969) as the ratio between the lateral earth pressure, σ_h, and the vertical pressure, σ_v. Moreover, the difference between the earth pressure coefficient from the simulation and that from Rankine's earth pressure theory is discussed (Lambe & Whitman, 1969). The earth pressure coefficient above the excavation surface along the rigid cylindrical shaft (10

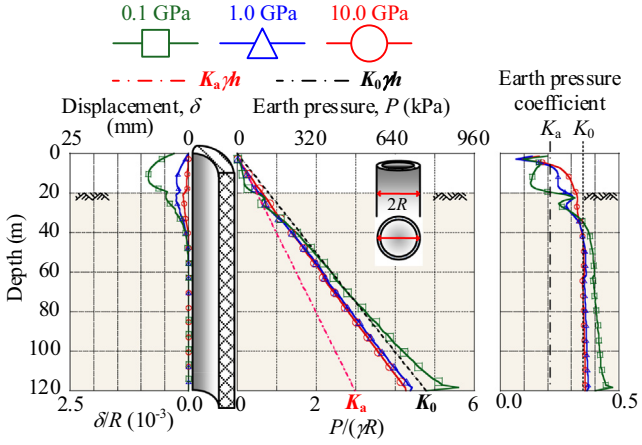

Fig. 10. Inner displacement and lateral earth pressure at 1st step of excavation (20 m).

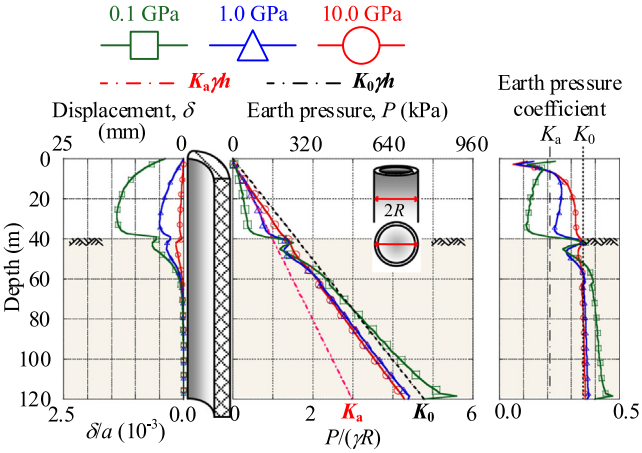

Fig. 11. Inner displacement and lateral earth pressure at 2nd step of excavation (40 m).

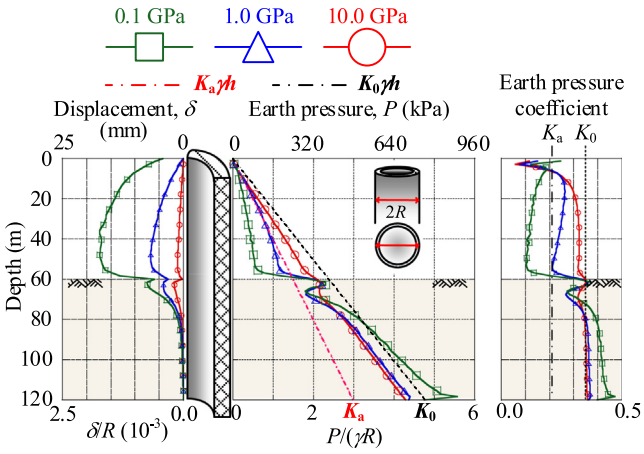

Fig. 12. Inner displacement and lateral earth pressure at 3rd step of excavation (60 m).

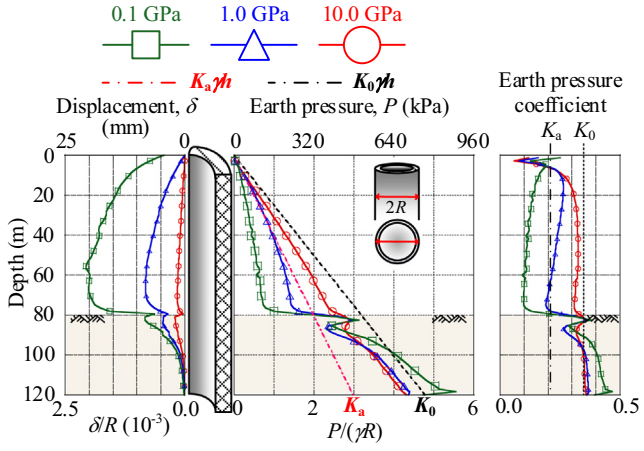

Fig 13. Inner displacement and lateral earth pressure at 4th step of excavation (80 m).

GPa) is relatively constant. Conversely, the others (0.1 GPa and 1 GPa) show a different tendency that the earth pressure coefficient above the excavation surface decreases in the depth direction.

These results show the unfamiliar mechanical behavior of the lateral earth pressure and the lateral displacement pattern. In addition, there are several obscure points which can be summarized as follows:

(1) There is a coherent relationship among the lateral earth pressure, the shaft deformation, and the shaft stiffness. Therefore, not only do the soil properties influence the lateral earth pressure, but they influence the shaft stiffness as well. As shown in the fundamental behavior results, the maximum displacement is generally located at a typical depth of 5 to 10 m above the excavation surface.

(2) In addition, the excavation process induces differences in the mechanical behavior of the earth pressure and the shaft deformation.

(3) The lateral earth pressure does not follow the active earth pressure theory, which is generally used for continuous retaining walls. Therefore, a general theory for the retaining wall design (a 2D solution) could not be applied to the cylindrical shaft design. According to the cylindrical structure and the unfamiliar lateral earth pressure (different from the 2D design), the arching effect may occur due to the inner displacement of the shaft wall. Therefore, the arching effect surrounding a circular shaft must be investigated.

(4) Looking at the results, the lateral earth pressure coefficient seems to be uncertain. Additionally, the earth pressure coefficient above the excavation surface has a tendency to decrease at deeper locations.

(5) According to the deep excavation, the effect of the depth might influence the development of different levels of earth pressure. The forced displacement method was applied in round shaft model tests, and the earth pressure at deeper locations seemed to be constant (Herten & Pulsfort, 1999; Tobar & Meguid, 2009; Tobar & Meguid, 2011). Moreover, the centrifuge tests of Iglesia et al. (2014) showed that the arching effect, occurring during the trapdoor experiments, brought about the transfer of pressure in the tangential direction, due to the displacement, and caused a decrease in earth pressure in the radial direction (Iglesia et al., 2014). In addition, the decrease in earth pressure from the arching effect was seen to decrease with incremental displacement as well. Therefore, the effect of depth on the trapdoor arching issue could imply horizontal arching along the cylindrical shaft.

3.2 Maximum displacement and minimum earth pressure coefficient of cylindrical shaft after excavation

According to cylindrical shaft structure, there are four main factors: (1) Lateral earth pressure, (2) Inner displacement, (3) Internal friction angle of soil, and (4) Shaft stiffness, influencing on the mechanical behavior of structure. The induction of changes in lateral earth pressure was examined by determining the influencing parameters. It is well known that the lateral earth pressure acting on the underground structure mainly depends on the internal friction angle, ϕ, of the soil and the allowance displacement or the inner displacement of the shaft, δ (Yu, 2011). Furthermore, the inner displacement of the shaft is related to the structural stiffness, which was shown in the previous analysis (Fundamental behavior of cylindrical vertical shaft during the excavation process). The maximum displacement (inner displacement) is generally taken into consideration in the design criteria and, in addition, there is a complicated relationship among the cylindrical shaft deformation (maximum displacement), the soil properties (internal friction angle), and the structural stiffness. Therefore, a 3D contour plot, composed of 256 analysis cases where Young's modulus of shaft and internal friction angle of soil varied as in Table 3, will be used to show the development of the maximum displacement and the average earth pressure coefficient above the excavation surface, as presented in Fig. 14.

According to the MCC model, the internal friction angle could not be directly assigned. The frictional constant, M, is the confining and deviatoric stress dependency or the ratio of the deviatoric stress to the mean effective stress, q/p_{cr}, at the critical state line, which will be represented instead of the internal friction angle (Schofield & Wroth, 1968; Itasca Consulting Group, 2017). The estimation of the frictional constant can be calculated as in Eq. (8) and Eq. (9) based on triaxial compression and triaxial extension tests, respectively (Wood, 1990; Itasca Consulting Group, 2017). The arching phenomenon basically undergoes both compression and extension. Moreover, the frictional constant representing arching cannot be calculated. According to the triaxial tests, either compression or extension is related to the change in only the major principal stress, σ_I, or the minor principal stress, σ_{III}. Hence, the frictional constant can be solved with the assumption that intermedi-

Table 3
Parametric study of shaft Young's modulus and internal friction angle of soil.

Young's modulus of shaft (Pa)	Internal friction angle of soil (°)
1.0×10^8	30
$10^{1/5} \times (1.0 \times 10^8)$	31
$10^{2/5} \times (1.0 \times 10^8)$	32
$10^{3/5} \times (1.0 \times 10^8)$	33
$10^{4/5} \times (1.0 \times 10^8)$	34
1.0×10^9	35
$10^{1/5} \times (1.0 \times 10^9)$	36
$10^{2/5} \times (1.0 \times 10^9)$	37
$10^{3/5} \times (1.0 \times 10^9)$	38
$10^{4/5} \times (1.0 \times 10^9)$	39
1.0×10^{10}	40
$10^{1/5} \times (1.0 \times 10^{10})$	41
$10^{2/5} \times (1.0 \times 10^{10})$	42
$10^{3/5} \times (1.0 \times 10^{10})$	43
$10^{4/5} \times (1.0 \times 10^{10})$	44
1.0×10^{11}	45

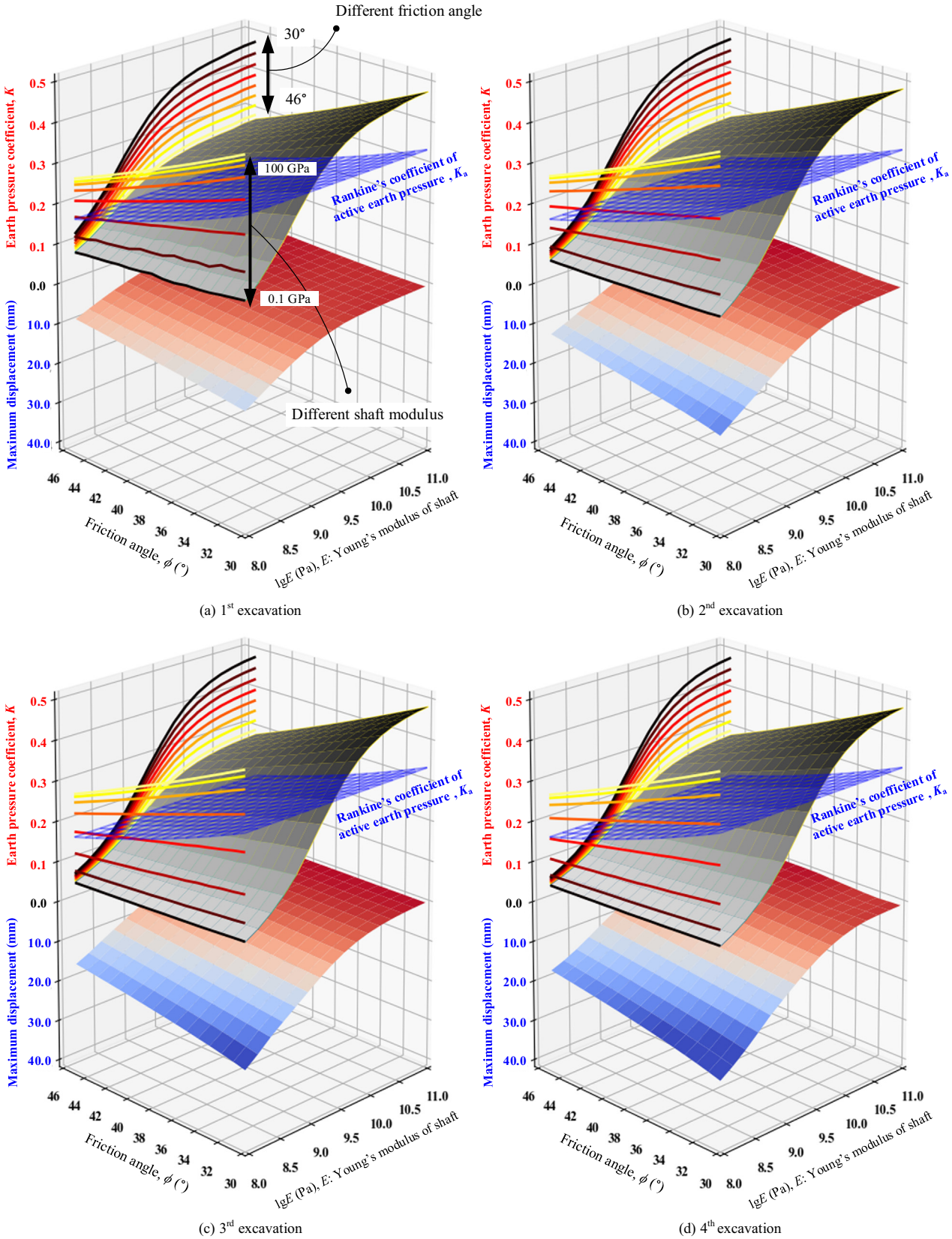

(a) 1st excavation

(b) 2nd excavation

(c) 3rd excavation

(d) 4th excavation

Fig. 14. Maximum displacement and average earth pressure coefficient above excavation surface.

ate principal stress σ_{II} remains the same with the minor or major principal stress. Conversely, if the arching effect, including both compression and extension, is considered in the failure analysis, the frictional constant cannot be analytically solved due to the additional unknown, namely, the major or minor principal stress. Therefore, the average value of the frictional constant, $\frac{M_c+M_t}{2}$, will be assigned as the MCC model parameter in accordance with the mechanical behavior of the arching effect, which includes compression and extension in the tangential and radial directions, respectively. In addition, Fig. 15 shows a comparison of the frictional constants calculated by compression and extension triaxial tests and the difference become larger as the friction angle increases. Moreover, the initial stress at the beginning, before carrying out the self-weight analysis, must be changed due to the variation in the frictional constant or the internal friction angle, using the Jaky (1944) empirical relationship, as given in Eq. (10) (Das, 2013b; Michalowski, 2005).

$$M_c = \frac{6\sin\phi'}{3-\sin\phi'}, \tag{8}$$

$$M_t = \frac{6\sin\phi'}{3+\sin\phi'}, \tag{9}$$

$$K_0 = 1-\sin\phi', \tag{10}$$

where M_c and M_t are frictional constants obtained by triaxial compression and triaxial extension, respectively, ϕ' is an effective internal friction angle of soil, and K_0 is at-rest earth pressure coefficient.

The highest maximum displacement after the final (4^{th} step) excavation is about 25 mm or 2.5×10^{-3} in normalized displacement, which can be observed in the case of the lowest shaft stiffness and the lowest internal friction angle of the soil. The reduction in the shaft stiffness or the internal friction angle of the soil will increase the maximum inner displacement corresponding to the results. Similarly, the average earth pressure coefficient above the excavation surface decreases, while the shaft stiffness decreases or the friction angle increases. Furthermore, it is very obvious that the generation of earth pressure surrounding the cylindrical shaft could not be estimated using a conventional theory considering the 2D problem.

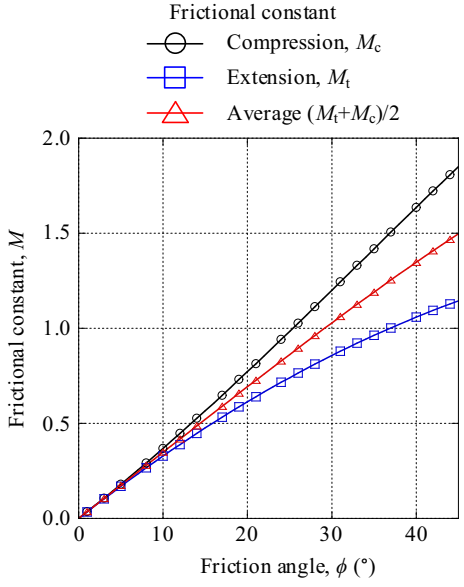

Fig. 15. Relationship between friction angle and frictional constant.

4 Results and discussion on ground arching effect on the cylindrical shaft

The results of the parametric study in the previous analysis are shown along with several sets of parameters, which could provide some tentative characteristics of the cylindrical shaft during excavation. Further analysis, employing the cylindrical shaft and soil parameters given in Tables 1 and 2, respectively, will enable the clarification of the mechanical behavior of the surrounding soil.

4.1 Generation of arching zone surrounding circular vertical shaft

The arching effect might be a cause of the generation of lateral earth pressure during wall deformation due to the excavation of the inside shaft in consonance with the cylinder structure and unfamiliar earth pressure, as in the previous results, especially in the case of a flexible (soft) cylindrical shaft. Therefore, an investigation of the arching effect on the surrounding shaft is necessary to comprehend the mechanical behavior of the surrounding soil.

Lee et al. (2006) clarified the arching effect due to a tunneling excavation using the arching ratio, $AR = \frac{\Delta\sigma_v}{\sigma_{v0}} \times 100\%$, where $\Delta\sigma_v$ is the change in vertical stress and σ_{v0} is the total vertical stress. The transferring load alongside a spring line is therefore parallel to the vertical direction (Lee et al., 2006). Pardo and Sáez (2014) performed a numerical modeling of the trapdoor to show the direction of load transfer, which is defined as the major principal stress direction (Pardo & Sáez, 2014). Barton and Bakhtar (1983) monitored the tangential stress in a cylindrical shaft lining, where the wall displacement and the tangential stress simultaneously increased. Similarly, the load transferring along the deformed cylindrical shaft occurred in a tangential direction, which caused a reduction in radial stress (Barton & Bakhtar, 1983).

According to the characteristics of the arching effect, the tangential stress will increase, while the radial stress will decrease, as shown in Fig. 16(a). Hence, the tangential stress ratio, $\frac{\sigma_{tt(current)}}{\sigma_{tt(initial)}}$, can confirm the existence of an arching zone surrounding the cylindrical shaft after the excavation process. The simulation of a flexible (soft) cylindrical shaft was chosen to show the arching effect along the cylindrical shaft after the excavation process. Furthermore, the results in Fig. 16(b) show the obvious development of an arching zone, following the excavation steps, and the tangential stress ratio also decreases in the radial direction.

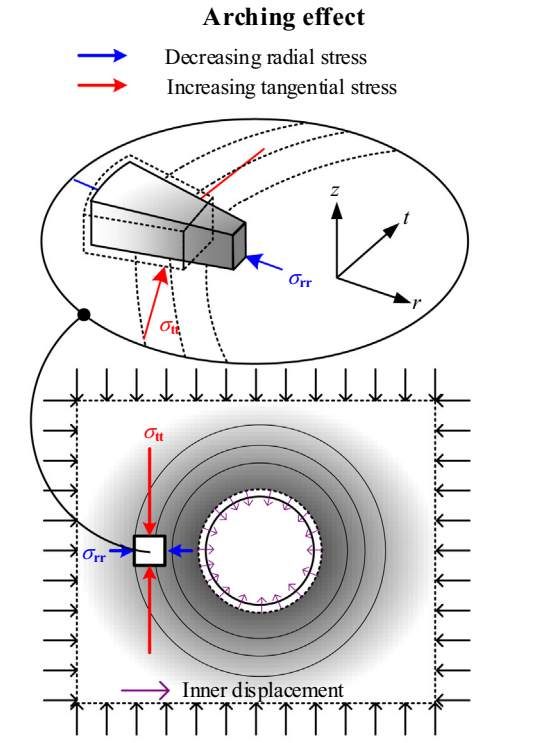

(a) Characteristic of arching effect

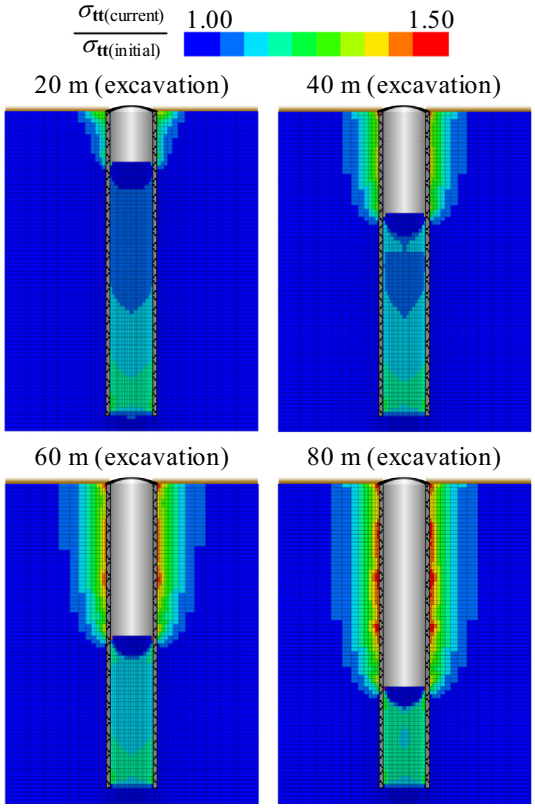

(b) Tangential stress contour

Fig. 16. Tangential stress ratio contour (100 MPa).

Figure 17 shows a comparison of the arching zone surrounding the cylindrical shaft after the final excavation step using the three different levels of shaft stiffness. According

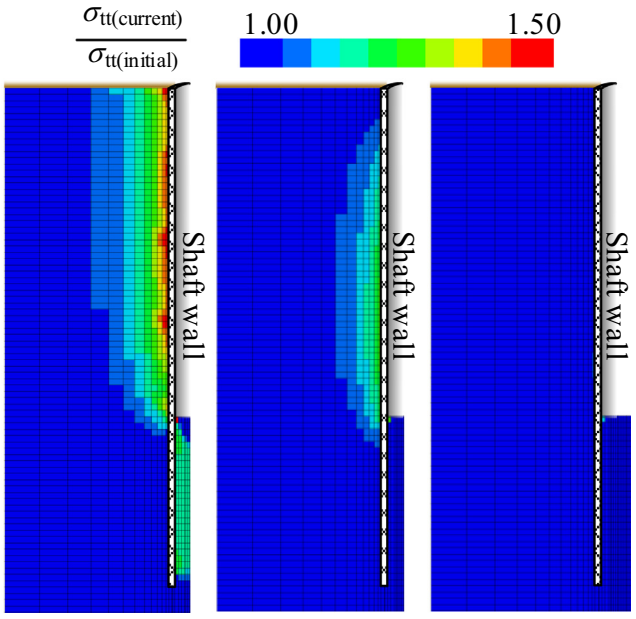

(a) 100MPa (b) 1GPa (c) 10GPa

Fig. 17. Contour of tangential stress ratio at final step of excavation (80 m).

to the results, the arching zone is obvious in the case of the flexible shaft (100 MPa), but it is relatively ambiguous in the case of the rigid shaft (10 GPa). In addition, the stress history in both radial and tangential directions confirmed the mechanism of the arching effect, as shown in Fig. 18. The stress history results show that the radial stress falls below the initial stress, while the tangential stress rises above the initial stress. According to the stress history, the radial stress immediately dropped due to the excavation. Then, the soil was allowed to displace in the radial direction in accordance with the reduction in radial stress. The tangential stress will eventually increase due to the inclination of the tangential strain from the soil deformation toward the shaft.

4.2 Strain ratio (ε_{radial} / $\varepsilon_{tangential}$) of surrounding soil after excavation

The earth pressure coefficient of the surrounding soil is uncertain, as shown in Figs. 10 to 13, even though the mechanical soil behavior, such as the arching effect, surrounding the cylindrical shaft can be defined. In addition, the strain will change in both radial and tangential directions, depending on both the arching effect and the stress generation. Therefore, the strain ratio of the radial strain and the tangential strain, $\varepsilon_{radial}/\varepsilon_{tangential}$, can be used to clarify particular characteristics of the arching soil surrounding the cylindrical shaft. The strain ratio of the surrounding soil will generally be a negative number in accordance with the opposite direction of strain generation in the arching effect, as shown in Fig. 19.

The strain ratio contours are given in Figs. 20 to 22 for the three levels of shaft stiffness, respectively. According to

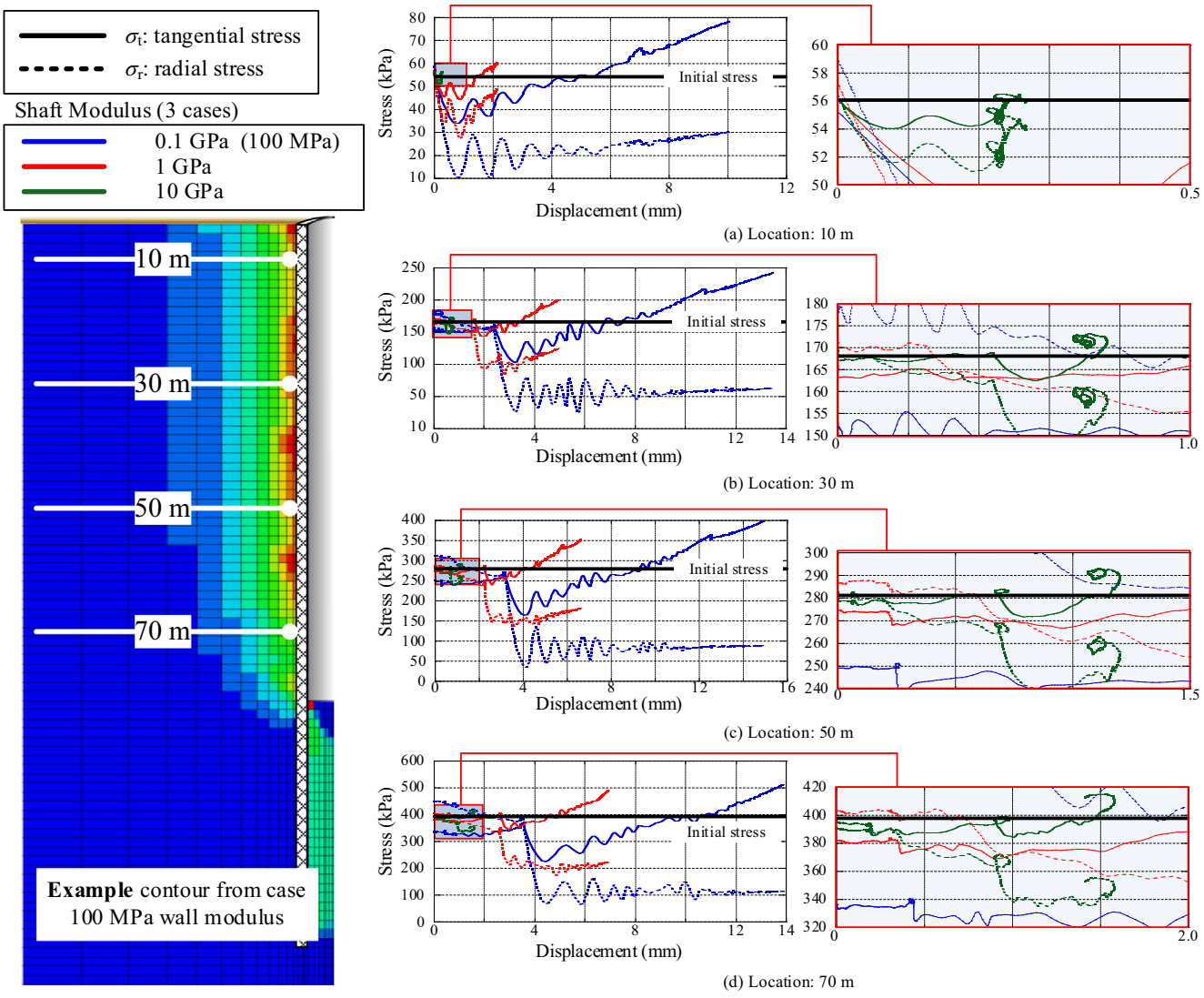

Fig. 18. Stress history of soil along circular shaft.

the results, the strain ratio of the surrounding soil near the cylindrical shaft is very close to −1. This means that the radial strain and tangential strain are developing equally, but in different directions (compressive strain in the tangential direction and tensile strain in the radial direction).

Furthermore, the strain ratio of the soil column along the cylindrical shaft shows that the strain ratio is explicitly decreasing with depth, which corresponds to the decrease in the earth pressure coefficient, as shown in Fig. 23, especially in the cases of Young's moduli of the shaft of 100 MPa and 1 GPa. Therefore, the strain ratio implies a reduction in radial stress, which can be proven by using a unit-element analysis.

4.3 Elucidation of earth pressure generation using unit element analysis

It is necessary to observe the characteristics of the mechanical behavior of the surrounding soil in order to elucidate the arching effect along the cylindrical shaft. Depending on the soil undergoing the arching effect, the mechanical behavior of the soil is still obscure under certain conditions, as mentioned previously: (1) influence of the strain ratio, $\varepsilon_{radial}/\varepsilon_{tangential}$, and (2) depth effect. In addition, a definition of the strain ratio has been given in Fig. 24. The strain in both radial and tangential directions was applied in a unit-element analysis to imitate the arching effect. In addition, the boundary conditions were fixed in the vertical direction, y-direction, and free in both tangential and radial directions. Therefore, this section will show that the generation of stress in the soil, based on a unit-element analysis, depends on these two conditions to elucidate the uncertainty of the earth pressure coefficient.

Figures 24 and 25 show the influences of the initial earth pressure on the stress generation in a low strain analysis for arching soil with OCR1 and OCR2, respectively. The maximum strain generation in this analysis is determined to correspond to the maximum displacement in the fundamental results by using the displacement strain relationship, $d = R - R^* = R\varepsilon_{tt}$, as shown in Fig. 19. Depending

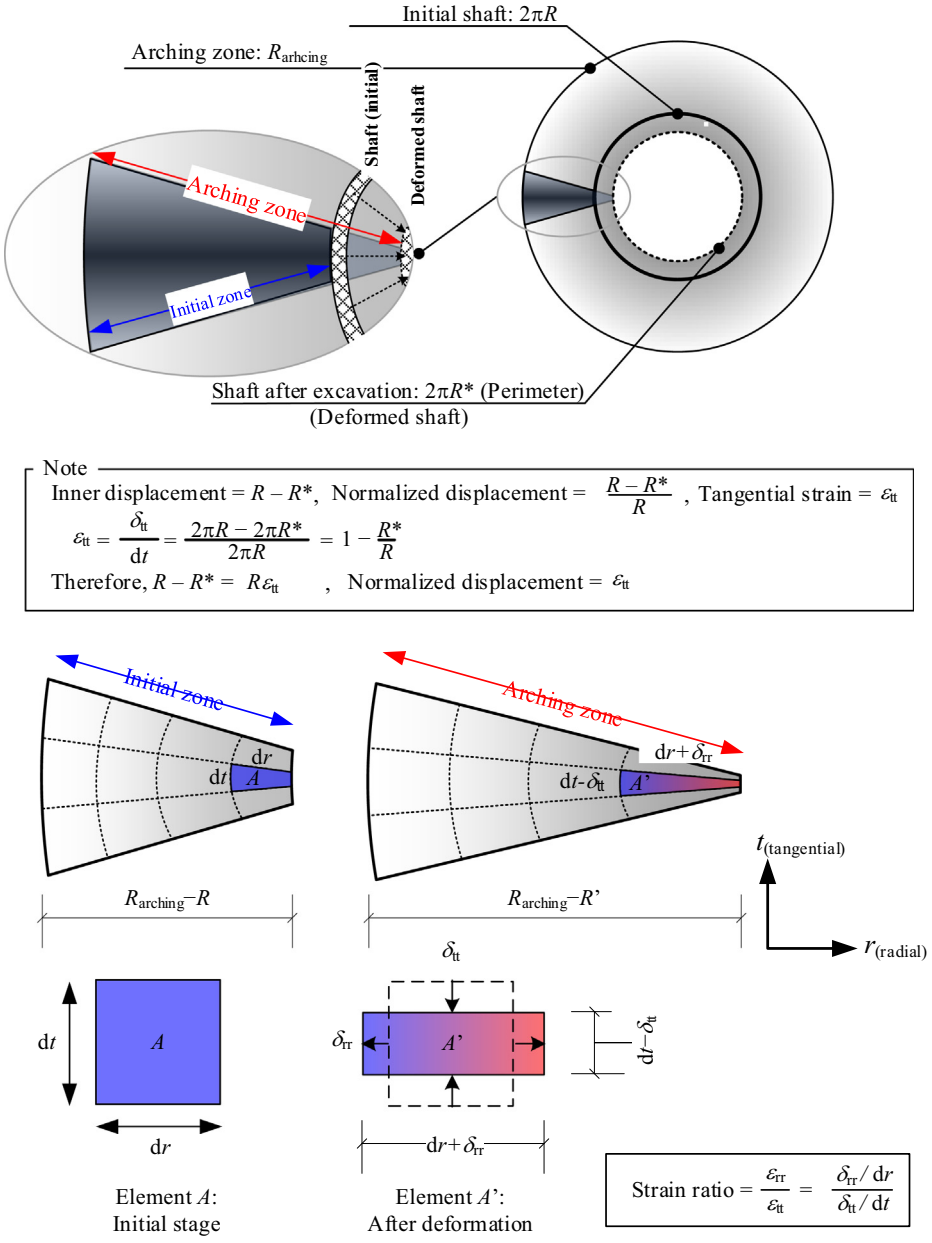

Fig. 19. Definition of strain ratio ($\varepsilon_{radial}/\varepsilon_{tangential}$).

on the deep cylindrical shaft construction, the different depths may be a main issue. Therefore, a comparison of the decrease in stress with several initial confining stress values will be shown to examine the stress reduction. The reduction in radial stress was greater in the case of higher initial confining stress than that in the case of lower confining stress, in accordance with the stress ratio results given in Figs. 24(b) and 25(b).

In addition, the stress generation influenced by the different strain ratios was examined to confirm the surrounding soil behavior in the previous analysis. Figures 26 and 27 show the generation of stress in the soil when applying different strain ratios, $\varepsilon_{radial}/\varepsilon_{tangential}$. The lower strain ratio can better reduce the radial stress than the others. For example, the reduction in radial stress in the case of a strain ratio of −0.6 is higher than that in the case of a strain ratio of −0.4, as shown in Figs. 26 (b) and 27(b). Therefore, these results correspond to the those of an uncertain earth pressure coefficient with increasing depth.

5 Comparison of numerical analysis with analytical solution

The earth pressure along the cylindrical shaft can be roughly estimated by an analytical solution commonly based on a specific assumption. Most of the analytical solution approaches have been based on slip-line and limit equilibrium methods without any consideration given to the wall deformation, such as those by Berezantzev (1958) and Prater (1977), respectively (Berezantev, 1958;

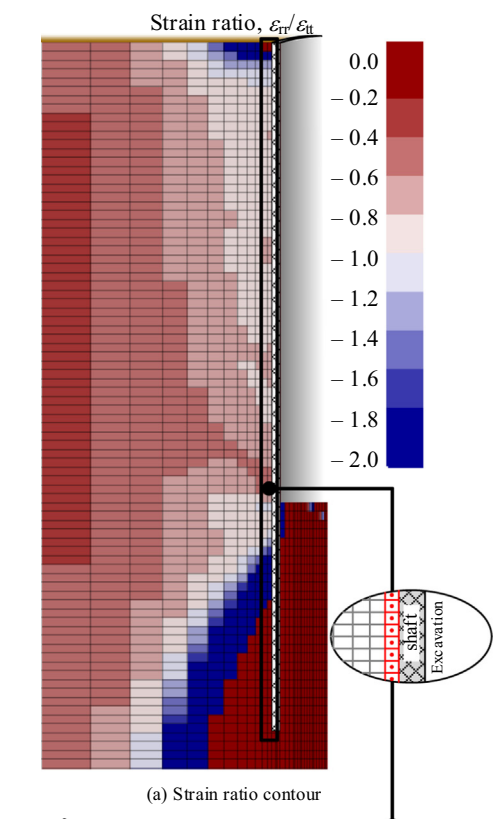

(a) Strain ratio contour

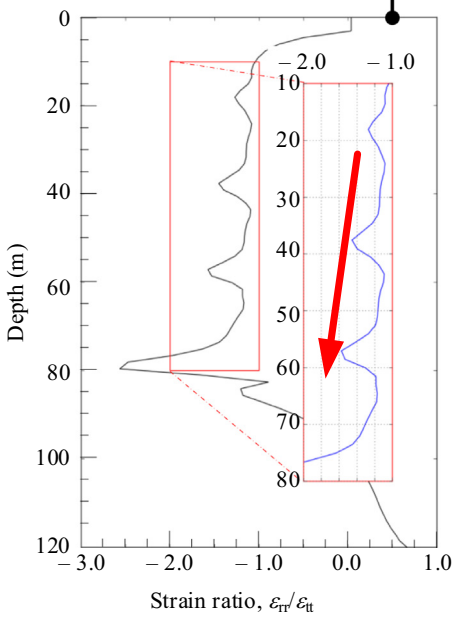

(b) Strain ratio of the soil column near shaft wall

Fig. 20. Strain ratio of surrounding soil (100 MPa).

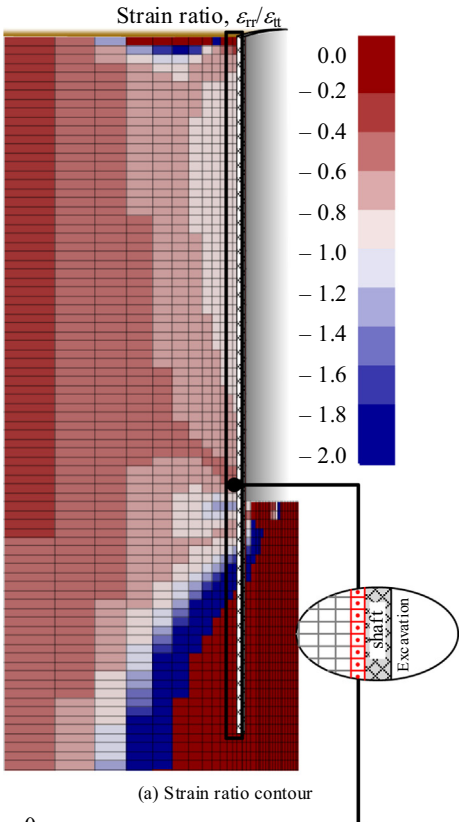

(a) Strain ratio contour

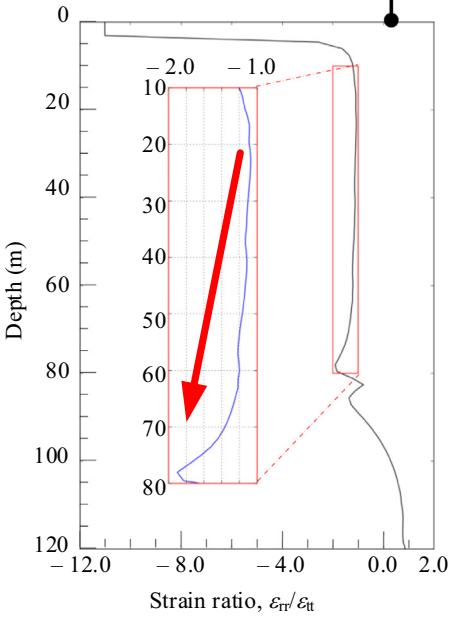

(b) Strain ratio of the soil column near shaft wall

Fig. 21. Strain ratio of surrounding soil (1 GPa).

Prater, 1977; Tobar & Meguid, 2010). The aim of these analytical solutions was to estimate the earth pressure acting on a cylindrical shaft after the excavation. Consequently, a comparison of the numerical analysis and the analytical solutions, as shown in Fig. 28, might be necessary. The various values of shaft stiffness, used for the comparison with the analytical solutions, are given in the Table 4.

Figure 28 shows that the earth pressure acting on a flexible (soft) vertical shaft is similar to the analytical solution of Cheng and Hu (2005), especially in the case where the Young's modulus is equal to $10^{3/5} \times 10^{8}$ Pa. Mostly, the earth pressure from the simulation results is relatively greater than that from the other analytical solutions. Recently, Cheng and Hu's solution has been the most prominent. The earth pressure at an excavation

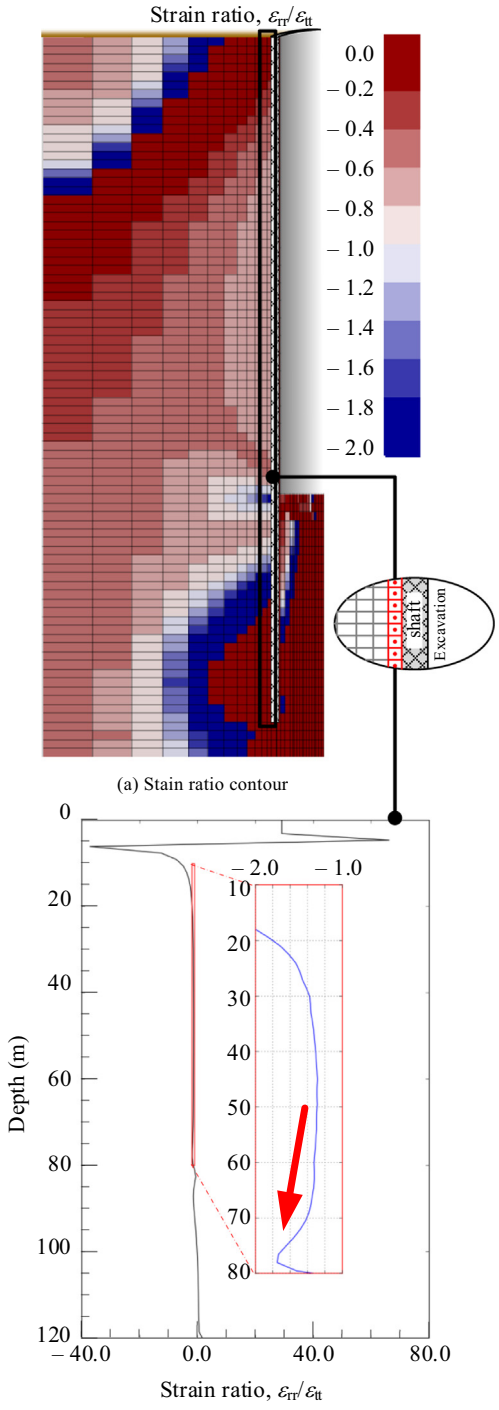

(a) Stain ratio contour

(b) Strain ratio of the soil column near shaft wall

Fig. 22. Strain ratio of surrounding soil (10 GPa).

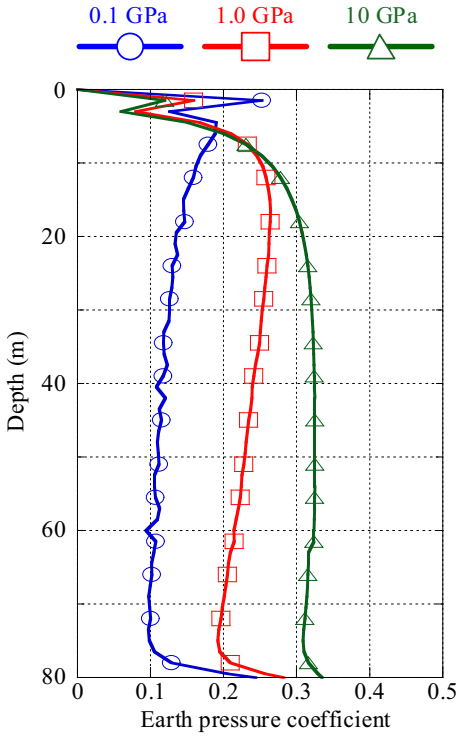

Fig. 23. Earth pressure coefficient after final excavation (80 m excavation).

site was taken for a comparison with that of Cheng and Hu (2005), as shown in Fig. 29. Cheng and Hu suggested an equation to estimate the earth pressure surrounding the cylindrical shaft; it is accompanied by the value presumed for the tangential pressure coefficient, λ as follows in Eq. (11). The value for the λ was assumed to fall in the range of K_a to 1.0 in agreement with Cheng and Hu's suggestion.

Figure 29 shows the earth pressure from Cheng and Hu's solution, with different values for λ and compares it with the simulation results. The earth pressure acting on a flexible (soft) cylindrical shaft is quite similar to the Cheng and Hu solution with large numbers for λ close to 1.0. Nevertheless, the earth pressure from the simulation results tends to be lower than the earth pressure from Chen and Hu at deeper locations.

$$P_a = r_0\gamma\frac{\sqrt{K_a}}{\eta-1}\left(1-\frac{1}{r_b^{\eta-1}}\right)+q\frac{1}{r_b^{\eta}}K_a - \cot\phi\left(\frac{1-\lambda+\eta}{\eta}-\frac{\varepsilon}{r_b}K_a\right)c, \tag{11}$$

where P_a is the earth pressure, r_0 is the shaft radius, C is the cohesion, q is the external surcharge, γ is the soil unit weight, h is the excavation depth, K_a is the active earth pressure coefficient, ϕ is the internal friction angle, $r_b = 1+\frac{h}{R}\sqrt{K_a}$, $\eta = \lambda\tan^2\left(45+\frac{\phi}{2}\right)-1$, and $\varepsilon = \frac{1-\lambda}{\eta}\tan^2\left(45+\frac{\phi}{2}\right)+1$.

However, the comparison as above could show only the similarity of earth pressure between analytical solution and numerical calculation, which is difficult to define suitable value of λ in the analytical solution to compare with each case of numerical simulation. Therefore, the analysis of correlation coefficient between analytical solution and numerical simulation data is performed here. Each numerical simulation result from Fig. 29, which was done under

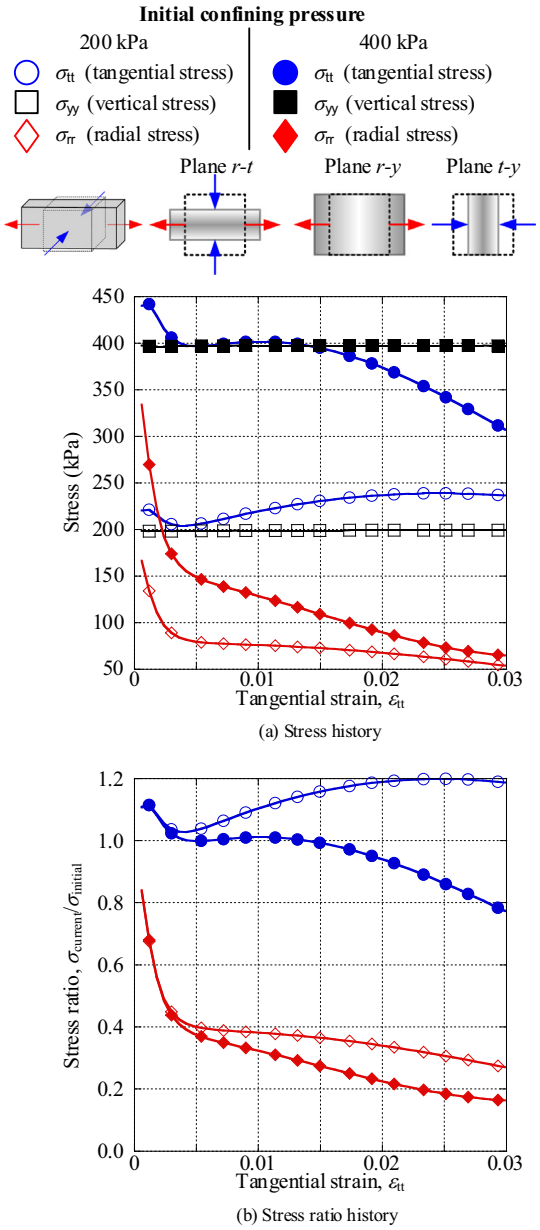

Fig. 24. Influence of confining pressure with OCR1 in unit-element analysis.

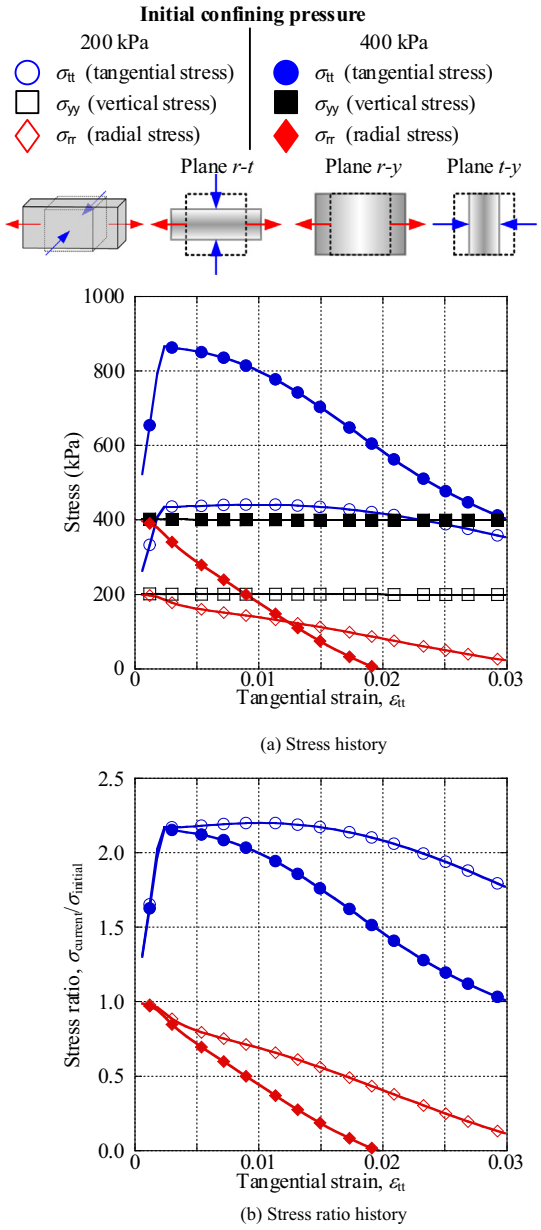

Fig. 25. Influence of confining pressure with OCR2 in unit-element analysis.

40°of internal friction angle, are compared with the 101 results of Cheng & Hu (2005) with different λ, in which the λ value is in the range [0,1] and gradually increased by 0.01 from 0 to 1. Subsequently, the maximum value of correlation coefficient from each case of numerical simulation is chosen and shown together with λ value as shown in Fig. 30. The correlation coefficient, r_{xy}, is calculated by using the dataset from numerical simulation and analytical solution, which are represented by x_i and y_i, respectively, as shown in Eq. (12).

$$r_{xy} = \frac{\sum_{i=1}^{n}(x_i - \bar{x})(y_i - \bar{y})}{\sqrt{\sum_{i=1}^{n}(x_i - \bar{x})^2}\sqrt{\sum_{i=1}^{n}(y_i - y)^2}} \quad (12)$$

Eventually, the correlation analysis result has additionally shown great correlation between the analytical solution and numerical simulation, especially in the case of Young's modulus of shaft greater than 1.0 GPa, as shown in Fig. 31. In addition, the result also shows the reduction of λ value, which is most correlated with numerical simulation, while the shaft displacement becomes larger.

6 Conclusion

Cylindrical shafts generally experience the arching effect due to the excavation sequences. The post-excavation earth

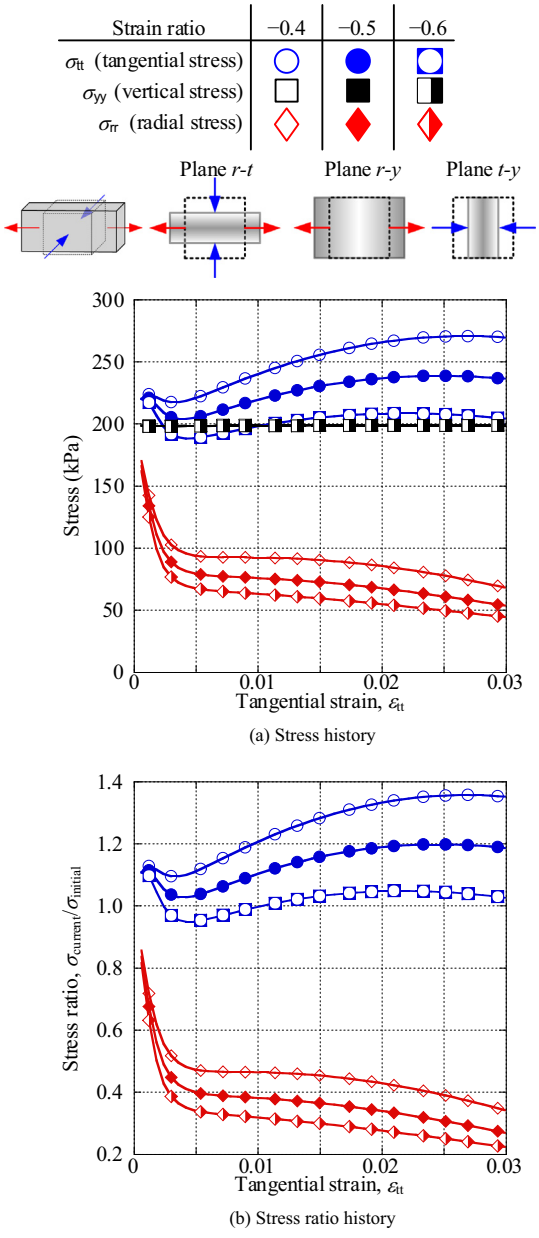

Fig. 26. Influence of strain ratio with OCR1 in unit-element analysis.

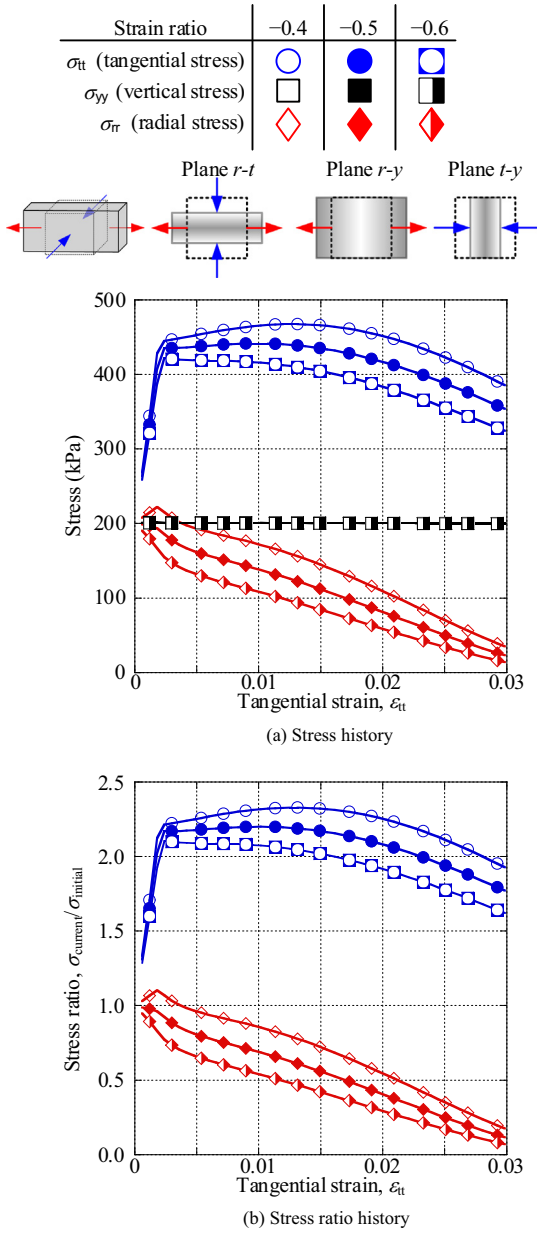

Fig. 27. Influence of strain ratio with OCR2 in unit- element analysis.

pressure on the cylindrical shaft, observed in this study, displayed an unusual tendency when compared to that observed with the theoretical solution obtained with Rankine's theory or the conventional earth pressure on a retaining wall structure. Furthermore, the translation mode (wall displacement) of a retaining wall (2D structure) is generally a rigid translation, whereas the displacement of a cylindrical shaft is the result of wall deformation. This is because the geometry of the cylindrical shaft brings about the occurrence of confining pressure, which prevents the cylindrical shaft from moving in any direction on the horizontal plane. Therefore, a two-dimensional analysis of the lateral earth pressure is not applicable for the earth pressure acting on a cylindrical shaft due to the additional direction of stress development, namely, compressive stress in a tangential direction.

The changes in the shaft deformation, lateral earth pressure, and shaft stiffness develop together, and thus, could not be separately considered. According to a three-dimensional plot of the maximum displacement, the shaft deformation will be better deformed when the shaft stiffness or the internal friction angle of the soil becomes lower. Another aspect that deserves attention is the earth pressure coefficient that develops together with the wall displacement, as shown in the 3-dimensional plot.

According to the partial excavation, the wall above the excavation surface is allowed to displace, causing a great reduction in earth pressure. Conversely, the earth pressure

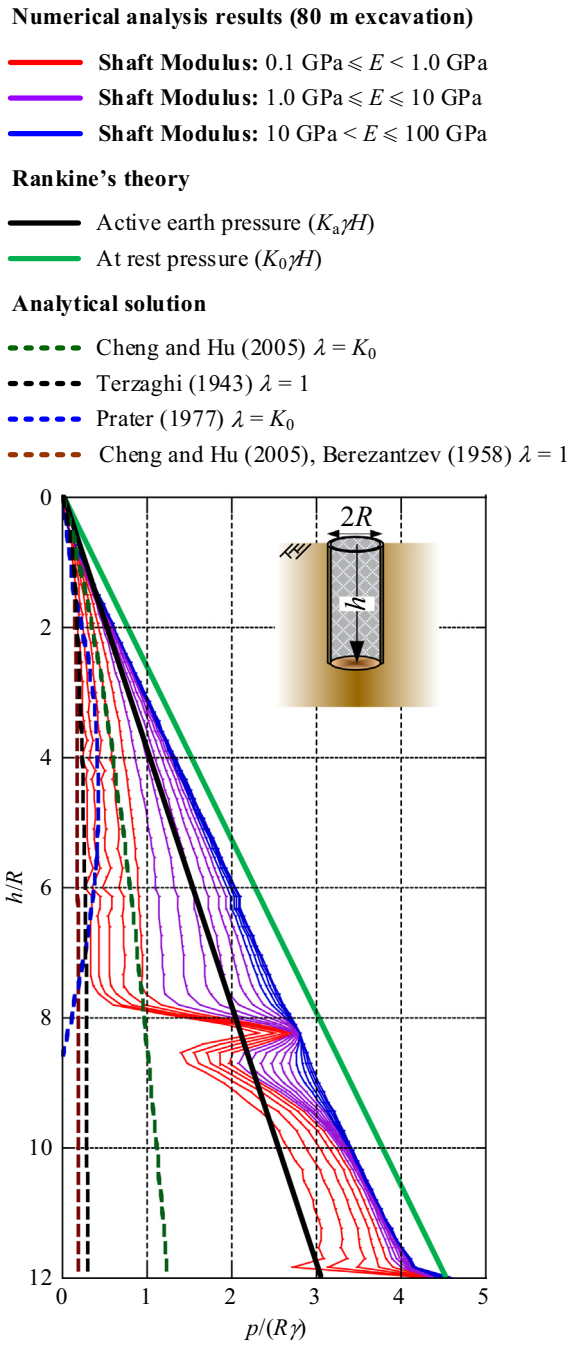

Fig. 28. Comparison of numerical analysis and analytical solutions.

near the excavation base rebounds back to the initial earth pressure due to the decreasing relative displacement.

The earth pressure coefficient above the excavation surface was seen to decrease with an increase in depth, although the mechanical behavior of the surrounding soil can be defined by the arching effect. The depth effect and the strain ratio, ε_{radial} /$\varepsilon_{tangential}$, play important roles in the reduction in earth pressure, which correspond to the earth pressure coefficient becoming lower when the depth becomes deeper. According to the unit-element analysis,

Table 4
Use of shaft stiffness in simulation.

Range of stiffness	Young's modulus, E (Pa)
0.1GPa ≤ E < 1.0GPa	1.0×10^8
	$10^{1/5}\times(1.0 \times 10^8)$
	$10^{2/5}\times(1.0 \times 10^8)$
	$10^{3/5}\times(1.0 \times 10^8)$
	$10^{4/5}\times(1.0 \times 10^8)$
1.0GPa ≤ E ≤ 10.0GPa	1.0×10^9
	$10^{1/5}\times(1.0 \times 10^9)$
	$10^{2/5}\times(1.0 \times 10^9)$
	$10^{3/5}\times(1.0 \times 10^9)$
	$10^{4/5}\times(1.0 \times 10^9)$
	1.0×10^{10}
10.0GPa < E ≤ 100.0GPa	$10^{1/5}\times(1.0 \times 10^{10})$
	$10^{2/5}\times(1.0 \times 10^{10})$
	$10^{3/5}\times(1.0 \times 10^{10})$
	$10^{4/5}\times(1.0 \times 10^{10})$
	1.0×10^{11}

the reduction in earth pressure at deeper positions and with higher confining pressure is basically lower than the reduction in earth pressure at shallower positions, which is mainly caused by the pressure dependency in the MCC model. On the other hand, the strain ratio decreases, while the depth increases, and the lower strain ratio normally shows a greater reduction in lateral earth pressure in correspondence with the unit-element analysis. However, a declination of the earth pressure coefficient with depth is observed. Hence, it might be concluded that the effect from the strain ratio reduction, which comes from the radial displacement, has a greater influence on the earth pressure coefficient than the effect from the pressure dependency at deeper positions.

A comparison among the various analytical solution and simulation results showed that the estimated lateral pressure from the analytical solution seems to be close to that of the flexible shaft simulation analysis or even more underestimated. Moreover, the analytical solution cannot assess the amount of lateral displacement either, as it is unable to consider the strain–stress relationship, $\frac{\partial \dot{\varepsilon}_\theta}{\partial r} - \frac{\dot{\varepsilon}_r - \dot{\varepsilon}_\theta}{r} = f_r$, due to the difficulty of including this additional consideration. Therefore, it leads to being incapable of earth pressure estimation with various levels of shaft stiffness.

In comparing the analytical solution from Cheng and Hu (2005) with the numerical simulation results, a similarity was found between the earth pressure acting on a flexible (soft) cylindrical shaft and the analytical solution results, with a high number for the tangential earth pressure coefficient, λ, which is in agreement with the numerical simulation results, for which the tangential stress ratio of the surrounding soil in the case of flexible (soft) cylindrical shaft tends to be high. Nevertheless, the earth pressure tendency from the numerical simulation did not correspond perfectly with that of the analytical solution, especially when the focusing location became deeper.

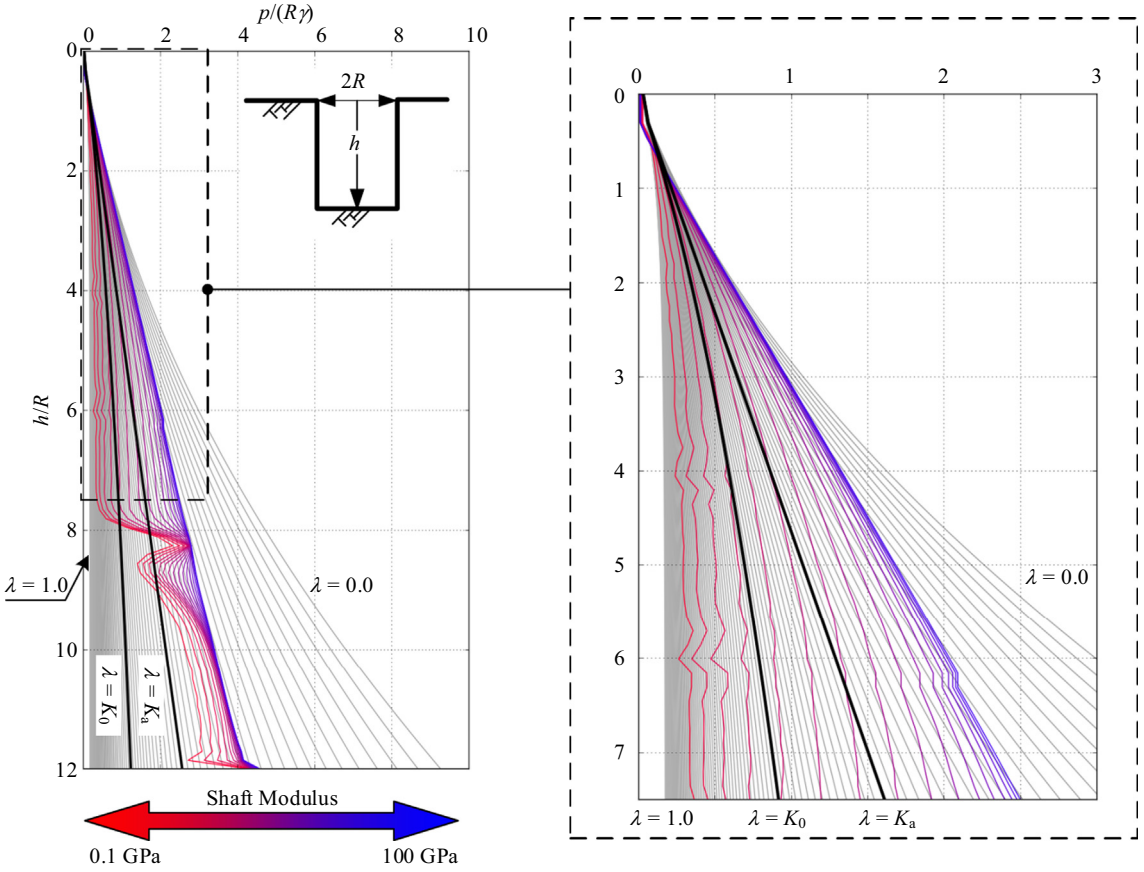

Fig. 29. Comparison of numerical analysis with Cheng and Hu (2005).

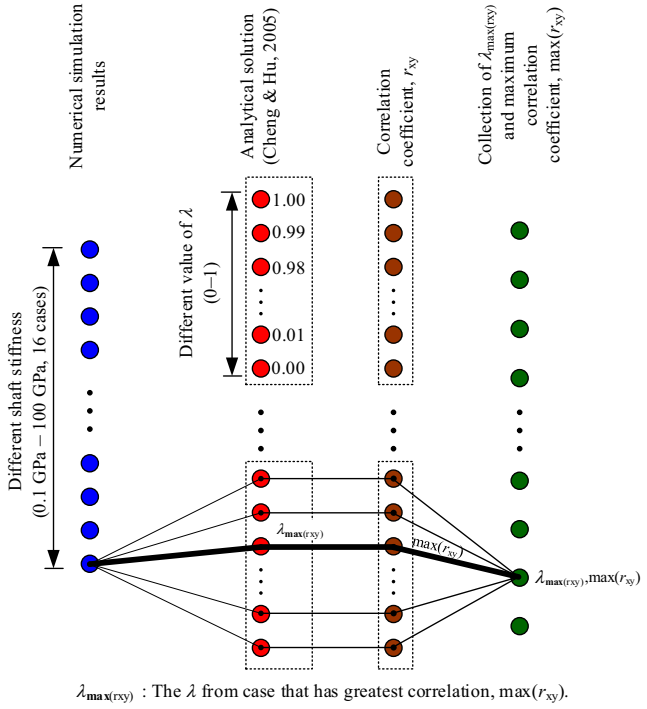

Fig. 30. Procedure for correlation analysis of data between numerical simulation and analytical solution.

The earth pressure along the cylindrical shaft changes due to the excavation, which is associated with the arching effect. The horizontal arching effect is very obviously observed along cylindrical shaft surface. The arching effect in the vertical direction, which is still obscure, might be another incentive of lateral earth pressure development.

The comparison between analytical solution and numerical simulation based on correlation rate coefficient shows the interesting point which could be future work for analytical solution. According to the comparison, the simulation result from the case of lower shaft stiffness, where large displacement generally occurs, has a great correlation with the analytical solution with higher value of λ. Conversely, the earth pressure from the case of small displacement of shaft wall is similar with the result of analytical solution with lower value of λ.

This research work mainly discussed a parametric study on a numerical model simulation and the relation between the numerical simulation and the analytical solution method. However, physical model tests are still necessary so that both the analytical method and the numerical model can be further validated. In particular, for deep cylindrical shaft problems, the depth effect plays a key role in the estimation. Therefore, simplified physical model tests on a deep cylindrical shaft might be very necessary for future research work.

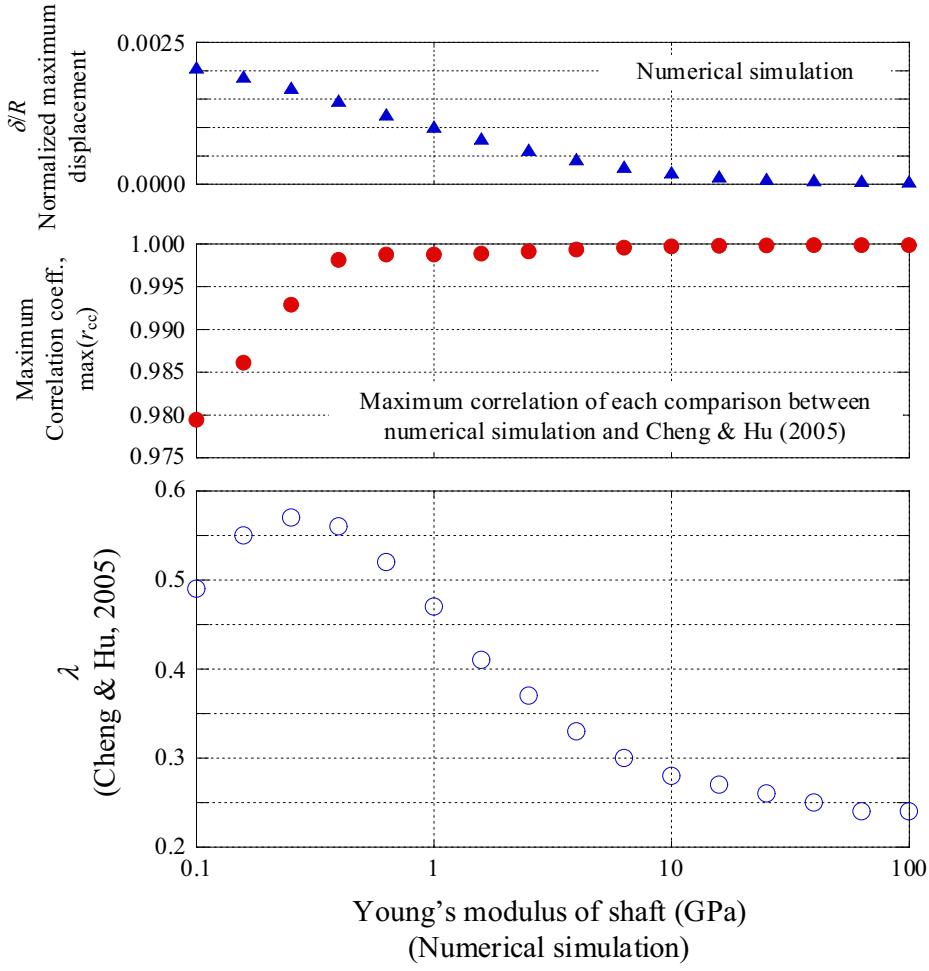

Fig. 31. Correlation between simulation result and analytical solution from Cheng and Hu (2005).

CRediT authorship contribution statement

Tanawat Tangjarusritaratorn: Exploration; Conceptualization; Methodology; writing-original draft. **Yuusuke Miyazaki:** Conceptualization; Methodology; editing. **Yasuo Sawamura:** Supervision. **Kiyoshi Kishida:** Administration; Resources; Visualization; Conceptualization; Supervision. **Makoto Kimura:** Supervision.

Declaration of Competing Interest

The authors declare that they have no known competing financial interests or personal relationships that could have appeared to influence the work reported in this paper.

Acknowledgements

This research work was partly supported by Association for Disaster Prevention Research.

References

Aglipay, M. R., Konagai, K., Kiyota, T., & Kyokawa, H. (2015). Simple Expression of the Ultimate Lateral Resistance of Piles on Sand based on Active Pile Length. *Journal of Japan Society of Civil Engineers, Ser. A1 (Structural Engineering & Earthquake Engineering (SE/EE))*, (4), I_329–I_336.

Aye, T. T., Tong, M. S. Y., Yi, K. H., & Arunasoruban, E. (2014). *Design and Construction of Large Diameter circular shafts*. Singapore: *Underground Singapore*.

Barton, N., & Bakhtar, K. (1983). Instrumentation and analysis of a deep shaft in quartzite. *Proceedings of 24th US Symposium on Rock Mechanics, College Station*, Texas, 371–384.

Berezantev, V.G. (1958). Earth pressure on the cylindrical retaining wall. In: Proceeding, *Brussels Conference on Earth Pressure Problems*, 2, 21–27.

Bruce, D. A. (2000). *An Introduction to the Deep Soil Mixing Methods as Used in Geotechnical Applications*. United States. Federal Highway Administration. Office of Infrastructure Research and Development (Chapter 2).

Bruce, M. E. C. & Geotechnica, Sa., Inc. (2013a). *Federal Highway Administration Design Manual: Deep Mixing for Embankment and Foundation Support*. McLean, VA : U.S. Department of Transportation, Federal Highway Administration, Research, Development, and Technology, Turner-Fairbank Highway Research Center (Chapter 3).

Bruce, M. E. C. & Geotechnica, Sa., Inc. (2013b). *Federal Highway Administration Design Manual: Deep Mixing for Embankment and Foundation Support*. McLean, VA: U.S. Department of Transportation, Federal Highway Administration, Research, Development, and Technology, Turner-Fairbank Highway Research Center, (Appendix A).

Chehadeh, A., Turan, A., Abed, F., & Yamin, M. (2019). Lateral earth pressures acting on circular shafts considering soil-structure interaction. *International Journal of Geotechnical Engineering, 13*(2), 139–151.

Cheng, Y. M., Hu, Y. Y., & Wei, W. B. (2007). General Axisymmetric Active Earth Pressure by Method of Characteristics—Theory and Numerical Formulation. *International Journal of Geomechanics, 7*(1), 1–15.

Cheng, Y. M., & Hu, Y. Y. (2005). Active earth pressure on circular shaft lining obtained by simplified slip line solution with general tangential stress coefficient. *Chinese Journal Geotechnical Engineering, 27*(1), 110–115 (in Chinese).

Cheng, Y. M., Wong, H., Leo, C. J., & Lau, C. K. (2016). *Stability of Geotechnical Structures: Theoretical and Numerical Analysis*. Bentham Science Publishers (Chapter 3).

Cho, J., Lim, H., Jeong, S., & Kim, K. (2015). Analysis of lateral earth pressure on a vertical circular shaft considering the 3D arching effect. *Tunnelling and Underground Space Technology, 48*, 11–19.

Das, B. M. (2013). *Principles of Geotechnical Engineering (7th ed.)*. Cengage Learning (Chapter 10).

Das, B. M. (2013). *Principles of Geotechnical Engineering (7th ed.)*. Cengage Learning (Chapter 13).

David, S., & Yang, R. (2003). Soil-cement walls for excavation support. *ADSC International Association of Foundation Drilling*, 1–17.

Dias, D., & Kastner, R. (2013). Movements caused by the excavation of tunnels using face pressurized shields — Analysis of monitoring and numerical modeling results. *Engineering Geology, 152*(1), 17–25.

Fan, J., Wang, D., & Qian, D. (2018). Soil-cement mixture properties and design considerations for reinforced excavation. *Journal of Rock Mechanics and Geotechnical Engineering, 10*(4), 791–797.

Fjar, E., Holt, Raaen, Risnes, R., & Horsrud, P. (2008). Petroleum Related Rock Mechanics. *Elsevier (Chapter*, 4).

Goh, K. H., & Mair, R. J. (2014). Response of framed buildings to excavation-induced movements. *Soils and Foundations, 54*(3), 250–268.

Handy, R. L. (1985). The Arch in Soil Arching. *Journal of Geotechnical Engineering, 111*(3), 302–318.

Hashash, Y. M. A., Marulanda, C., Ghaboussi, J., & Jung, S. (2003). Systematic update of a deep excavation model using field performance data. *Computers and Geotechnics, 30*(6), 477–488.

Herten, M., & Pulsfort, M. (1999). Determination of spatial earth pressure on circular shaft constructions. *Granular Matter, 2*(1), 1–7.

Hsieh, P.-G., Ou, C.-Y., & Lin, Y.-L. (2012). Three-dimensional numerical analysis of deep excavations with cross walls. *Acta Geotechnica, 8*(1), 33–48.

Iglesia, G. R., Einstein, H. H., & Whitman, R. V. (2014). Investigation of Soil Arching with Centrifuge Tests. *Journal of Geotechnical and Geoenvironmental Engineering*, *140*(2), 04013005.

Jaky, J. (1944). The coefficient of earth pressure at rest. *Journal of the Society of Hungarian Architects and Engineering*, 355–358.

Imamura, S., Nomoto, T., Fuji, T., & Hagiwara, T. (2000). Earth pressures acting on a deep shaft and the movements of adjacent ground in sand. *Geotechnical Aspects of Underground Construction in Soft Ground*, 647–652.

Itasca Consulting Group, Inc. (2017). FLAC3D - Fast Lagrangian Analysis of Continua in Three-Dimensions. Ver.6.0. Minneapolis: Itasca.

Jiang, Y., Han, J., & Zheng, G. (2013). Numerical analysis of a pile–slab-supported railway embankment. *Acta Geotechnica, 9*(3), 499–511.

Kim, K.-Y., Lee, D.-S., Cho, J., Jeong, S.-S., & Lee, S. (2013). The effect of arching pressure on a vertical circular shaft. *Tunnelling and Underground Space Technology, 37*, 10–21.

Lai, H.-J., Zheng, J.-J., Zhang, R.-J., & Cui, M.-J. (2018). Classification and characteristics of soil arching structures in pile-supported embankments. *Computers and Geotechnics, 98*, 153–171.

Lambe, T. W., & Whitman, R. V. (1969). *Soil Mechanics*. New York: John Wiley & Sons.

Lee, C. J., Wu, B. R., Chen, H. T., & Chiang, K. H. (2006). Tunnel stability and arching effects during tunneling in soft clayey soil. *Tunnelling and Underground Space Technology, 21*(2), 119–132.

Liu, F. Q. (2014). Lateral earth pressures acting on circular retaining walls. *International Journal of Geomechanics, 14*(3), 04014002.

Liu, F. Q., & Wang, J. H. (2008). A generalized slip line solution to the active earth pressure on circular retaining walls. *Computers and Geotechnics, 35*(2), 155–164.

Meftah, A., Benmebarek, N., & Benmebarek, S. (2018). Numerical study of the active earth pressure distribution on cylindrical shafts using 2D finite difference code. *Journal of Applied Engineering Science & Technology, 4*(2), 123–128.

Michalowski, R. L. (2005). Coefficient of Earth Pressure at Rest. *Journal of Geotechnical and Geoenvironmental Engineering, 131*(11), 1429–1433.

Muramatsu, M., & Abe, T. (1996). *Considerations in shaft excavation and peripheral ground deformation*. Balkema, Rotterdam: Geotechnica/ Aspects of Underground Construction in Soft Ground.

Nakai, T., Shahin, H. Md, Kikumoto, M., Kyokawa, H., Zhang, F., & Farias, M. M. (2011). A Simple and Unified Three-Dimensional Model to Describe Various Characteristics of Soils. *Soils and Foundations, 51*(6), 1149–1168.

Nakai, T., Xu, L., & Yamazaki, H. (1997). 3D and 2D Model Tests and Numerical Analyses of Settlements and Earth Pressures Due to Tunnel Excavation. *Soils and Foundations, 37*(3), 31–42.

Ng, C., Fong, K., & Liu, H. (2018). The effects of existing horseshoe-shaped tunnel sizes on circular crossing tunnel interactions: Three-dimensional numerical analyses. *Tunnelling and Underground Space Technology, 77*, 68–79.

Nunez, M. A., Briançon, L., & Dias, D. (2013). Analyses of a pile-supported embankment over soft clay: Full-scale experiment, analytical and numerical approaches. *Engineering Geology, 153*, 53–67.

Paik, K. H., & Salgado, R. (2003). Estimation of active earth pressure against rigid retaining walls considering arching effects. *Géotechnique, 53*(7), 643–653.

Pardo, G. S., & Sáez, E. (2014). Experimental and numerical study of arching soil effect in coarse sand. *Computers and Geotechnics, 57*, 75–84.

Prater, E. G. (1977). An examination of some theories of earth pressure on shaft linings. *Canadian Geotechnical Journal, 14*(1), 91–106.

Rui, R., van Tol, F., Xia, Y. Y., van Eekelen, S., & Hu, G. (2018). Evolution of Soil Arching: 2D Analytical Models. *International Journal of Geomechanics, 18*(6), 04018056.

Salman, F. A., Fattah, M. Y., & Sabre, D. K. (2011). Long term behavior of a retaining wall resting on clayey soil. *International Journal of the Physical Sciences, 6*(4), 730–746.

Schofield, A. N., & Wroth, P. (1968). *Critical State Soil Mechanics*. Mcgraw-Hill (Chapter 6).

Sun, Q. Q., & Dias, D. (2019). Assessment of stress relief during excavation on the seismic tunnel response by the pseudo-static method. *Soil Dynamics and Earthquake Engineering, 117*, 384–397.

Tan, Y., & Wang, D. (2013). Characteristics of a Large-Scale Deep Foundation Pit Excavated by the Central-Island Technique in Shanghai Soft Clay. I: Bottom-Up Construction of the Central Cylindrical Shaft. *Journal of Geotechnical and Geoenvironmental Engineering, 139*(11), 1875–1893.

Tan, Y., Lu, Y., Xu, C., & Wang, D. (2018). Investigation on performance of a large circular pit-in-pit excavation in clay-gravel-cobble mixed strata. *Tunnelling and Underground Space Technology, 79*, 356–374.

Tang, L., Cong, S., Xing, W., Ling, X., Geng, L., Nie, Z., & Gan, F. (2018). Finite element analysis of lateral earth pressure on sheet pile walls. *Engineering Geology, 244*, 146–158.

Terzaghi, K., Chapman and Hall (Londyn)., & John Wiley & Sons. (1943a). Theoretical Soil Mechanics. Wiley (Chapter 10).

Terzaghi, K., Chapman and Hall (Londyn)., & John Wiley & Sons. (1943b). Theoretical Soil Mechanics. Wiley (Chapter 6).

Tobar, T., & Meguid, M. (2009). *Distribution of active earth pressure on vertical shafts*. Canadian Young Geotechnical Engineers and Geoscientist Conference, Halifax, NS.

Tobar, T., & Meguid, M. A. (2010). Comparative evaluation of methods to determine the earth pressure distribution on cylindrical shafts: A review. *Tunnelling and Underground Space Technology, 25*(2), 188–197.

Tobar, T., & Meguid, M. A. (2011). Experimental Study of the Earth Pressure Distribution on Cylindrical Shafts. *Journal of Geotechnical and Geoenvironmental Engineering, 137*(11), 1121–1125.

Wood, D. M. (1990). *Soil Behaviour and Critical State Soil Mechanics*. Cambridge University Press (Chapter 7).

Xiong, G. J., Wang, J. H., & Chen, J. J. (2019). Theory and practical calculation method for axisymmetric active earth pressure based on the characteristics method considering the compatibility condition. *Applied Mathematical Modelling, 68*, 563–582.

Yu, W. L. (2011). Estimation of the active earth pressure with inclined cohesive backfills: the effect of intermediate principal stress is considered. *The Open Civil Engineering Journal, 5*(1), 9–16.

Zhang, B., & Chen, Z. (2019). Effects of nominal flexibility ratio and shaft dimensionless parameters on the seismic response characteristics of deep shafts. *Soil Dynamics and Earthquake Engineering, 20*, 257–261.